A REVIEW ON THE SEGOVIA BATHOLITH AND ITS THERMAL HISTORY, IMPLICATIONS FOR METALLOGENESIS IN THE SEGOVIA-REMEDIOS MINING DISTRICT

Elaborated by:

Andrea Malo Gonzalez

Bachelor thesis presented as required to obtain the title of Geologist

Thesis advisor:

Maria Isabel Marín Cerón

EAFIT University
School of Sciences
Earth Science Department
Medellín, Colombia
2020

CONTENTS

PREFACE

This study is presented as a manuscript to be submitted in the Journal of South American Earth Sciences. Additional material attached includes field notes, petrographic descriptions, and photographic support. The results presented are associated with the research production of the Economic Geology Research Group of EAFIT University.

I dedicate this work to my family for their infinite kindness, love, and care.

I gratefully acknowledge the financial and logistics support of Gran Colombia Gold in the development of this study, especially the geologists of the exploration program who accompanied the fieldwork: Alessandro Cecchi, Leonardo Santacruz, Gustavo Morales, Luis Paez, and Jorge Cardona.

I appreciate the direction of my advisor Dr. Maria Isabel Marin, for her patience and persistence. Special thanks to Gino Chuquimia, MSc. student at EAFIT, for his support and guidance, and Santiago Noriega, Ph.D. student at EAFIT, for his thoughtful recommendations.

Profound thanks to Dr. Camilo Bustamante and Dr. Sergio Restrepo for critically reviewing the manuscript for its improvement.

I am fortunate to have learned from amazing professors together with great colleagues and friends. Thanks to Liz, Richie, Sebas, and David for encouraging me throughout this work.

ABSTRACT

Assessing the thermal history of metalliferous districts via low-temperature thermochronology is key to understand metal transfer and ore exhumation processes in active orogens. Previous thermal models of the Segovia Batholith need revision using more recent thermochronological data in the light of current geodynamic models. This study reviews the geological characteristics of the Segovia Batholith using available data. One of the objectives aims at reconstructing the batholith's thermal history at regional and local scales in Gran Colombia Gold's Segovia Project. The Segovia Batholith covers ~1600 km^2 and is located in the northern Colombian Central Cordillera, structurally limited by the Otú and Palestina faults. The time-temperature trajectory constructed for this unit signals a Late Cretaceous-Paleocene exhumation event, coetaneous with early uplift of the proto-Central Cordillera, associated with a period of increased convergence between the Farallones, Caribbean, and South American plates. This period is contemporaneous with activation of the Otú Fault and mineralization timing of the Segovia-Remedios mining district. However, uplifting occurs asynchronously for different tectonic blocks. More rapid uplift west of the Otú Fault might have favored fluid migration from sub-cortical intrusions of the Antioquia Batholith towards the slow-exhuming Segovia Batholith to the east. At a local scale in the Segovia Project, the most prospective areas are located towards west close to the fluid source and permeable channel, between distensive areas of right-lateral shear with NW-SE-oriented compression, following R, R' and P secondary structures. Furthermore, elevated thermal gradients in distensive areas facilitates effective metal transfer and can host higher ore grades.

RESUMEN

Analizar la historia termal de distritos mineros usando termocronología de baja temperatura es clave para entender procesos de transferencia de metales y exhumación en orogenos activos. Modelos termales previos del batolito de Segovia necesitan ser revisados integrando datos termocronológicos recientes a la luz de modelos geodinámicos actuales. Se presenta una revisión de las características geológicas del Batolito de Segovia con datos disponibles a la fecha, con el objetivo de analizar su historia termal a escala regional y local en el proyecto Segovia de Gran Colombia Gold. El batolito de Segovia cubre ~1600 km^2 en el norte de la Cordillera Central Colombiana, limitado estructuralmente las fallas Otú y Palestina. La trayectoria tiempo-temperatura marca un evento de exhumación Cretácico Tardío-Paleoceno coetáneo con fases de levantamiento tempranas de la proto-Cordillera Central, asociadas a un periodo de convergencia aumentada entre las placas Farallones, Caribe, y Suramericana. Este periodo es contemporáneo con la activación de la falla Otú y la mineralización en el distrito minero Segovia-Remedios. La exhumación diferencial de bloques tectónicos favoreció la migración de fluidos hidrotermales provenientes de intrusiones sub-corticales del Batolito Antioqueño hacia el Batolito de Segovia con exhumación lenta. En el proyecto Segovia, las áreas más prospectivas se ubican al W cerca a la fuente de los fluidos y el canal de mineralización, entre zonas distensivas de una compresión NW-SE, siguiendo estructuras secundarias R, R' y P. Los altos gradientes termales en bloques distensivos del proyecto Segovia facilitan la transferencia efectiva de metales y pueden alojar mineralización de mayor tenor.

1. INTRODUCTION

Defining the areas with the greatest potential in metallic mineral districts requires a clear understanding of the numerous factors that control their formation, such as tectonic setting, fertile magmatism, structural configuration, and crustal thermal conditions (McInes et al., 2005; Wood and Hedenquist, 2019). However, determining the nature, timing, and relation of these factors with ore formation is no simple task, especially in regions with active orogenesis (Bernet et al., 2019). Assessing them through a multi-disciplinary, multi-tool approach seems the leading way in successful exploration, taking advantage of geochronological, geochemical, and thermochronological techniques (Bernet et al., 2019), combined with petrographical and structural analysis.

The Segovia-Remedios Mining District is located in the eastern flank of the Colombian Central Cordillera, and contains the most fertile Au-Ag deposits of the country (Oróñez et al., 2005; López et al., 2018; Shaw et al., 2019). The main operator in the district, Gran Colombia Gold, reports mineral reserves of 19 Mt at an average grade of 11.02 g/t Au in the Segovia Project (SRK Consulting, 2018), from which it produces gold-quartz veins hosted by the Jurassic Segovia Batholith.

A few studies have investigated the metallogenesis of the Segovia-Remedios district by analyzing different geological features. A strong structural control resemble characteristics of orogenic-type deposits (Ordóñez-Carmona et al., 2005; Rodríguez, 2007; Sánchez et al., 2007), but fluid inclusions analyses find physico-chemical properties probable for epithermal and intrusion-related deposits (Manco et al., 2012; Álvarez, 2013; Castaño-Dávila et al., 2019). Overlapping ore deposit features difficult assigning a unique classification. Notwithstanding, A Late Cretaceous age for the mineralization limits the role of the Segovia Batholith in gold genesis, acting only as its host rock (Leal-Mejía, 2011; López et al., 2018). Instead, the coetaneous and adjacent Antioquia Batholith, with its Cretaceous crystallization age (Restrepo-

Moreno, 2009; Duque-Trujillo et al., 2019; Leal-Mejía et al., 2019) is likely the source of metal fluids and heat in the Segovia-Remedios mining district (Echeverri, 2006; Leal-Mejía, 2011; Manco et al., 2012; Álvarez, 2013). However, the interaction of tectonomagmatic, structural, and thermal processes in the timing of fluid expulsion and concentration are still to comprehend.

Low-temperature thermochronology is a powerful technique to reconstruct the cooling and exhumation history of a mineral host rock, which is related to factors that control metal transfer and precipitation in the crust (McInes et al., 2005; Bernet et al., 2019). Echeverri (2006) constructed the thermal history of the Segovia Batholith using fission-track data and concluded that it cooled at low, steady rates in a quiescent tectonic environment, by means of post-magmatic heat loss all through its Jurassic-to-present evolution. However, current studies recognize several uplift phases in the Central Cordillera that reflect the Northern Andean Orogeny since the Late Cretaceous based on provenance (Horton et al., 2010), stratigraphic (Clavijo et al., 2008, Caballero et al., 2013), thermochronological (Villagomez and Spikings, 2013; Spikings et al., 2015), and morphometric (García-Delgado and Velandia, 2020) analyses. This study hypothesizes that the Segovia Batholith cooled via tectonic-driven exhumation responding to active tectonic shortening, with effects on the tempo and grade of gold mineralization.

As new investigations develop in the northern Central Cordillera, the significance and validity of previous metallogenetic models for the Segovia-Remedios Mining District need revision. This study compiles geological data of the Segovia Batholith to review its geochronological, geochemical, petrographic, and structural features, and uses available low-temperature thermochronological data to reconstruct its cooling history at regional and local scales. Using this information, this study analyses the spatiotemporal links between the tectonomagmatic evolution of the Northern Andes convergent margin and gold mineralization in the Segovia-

Remedios Mining District and questions at what extend the thermal configuration of the Segovia Batholith play a role in deposit formation in the Segovia Project.

2. REGIONAL GEOLOGICAL SETTING

Colombia has a distinct physiography characterized by three N-S-oriented cordilleras separated by intermontane valleys, namely the Eastern, Central, and Western cordilleras. The Eastern Cordillera is an inverted basin with Precambrian-Paleozoic metamorphic and igneous basement, covered by Paleozoic to Cenozoic sedimentary strata (Cediel et al., 2003; Sarmiento-Rojas et al., 2006; Villamil, 2011). To the west, the Magdalena River separates it from the Central Cordillera, made of a Proterozoic and Paleozoic metamorphic basement intruded by arc-related Jurassic and Cretaceous plutons (Feininger et al., 1972; Bustamante et al., 2016; Leal-Mejía et al., 2019). Further west, the Cauca River divides the Central and Western cordilleras. The latter comprises Cretaceous basaltic rocks originated in an intra-oceanic setting in the Caribbean plateau (Kerr et al., 1997), accreted to the continental margin from the Early Cretaceous to the middle Miocene (Kennan and Pindell, 2009; Spikings et al., 2015).

The early geodynamic evolution of the paleo Central Cordillera was dominated by convergence, first with the collision of Laurentia and Amazonia during the Grenville Orogeny about 1200 Ma (Cordani et al., 2005; Cuadros, 2012), and then with a Middle Ordovician-Silurian orogeny related to Pangea amalgamation (Cediel et al., 2003). The former assembled the basement of the Central Cordillera's eastern flank, made of exhumed granulite-grade migmatites and gneisses (Maya and González, 1995; Cuadros, 2012), and the latter formed the medium-grade polymetamorphic basement of the cordillera axis (Maya and González, 1995; Cediel et al., 2003). In the late Paleozoic, an extensional convergent regime was established associated with subduction onset of the Pacific Plate beneath the western South American Plate (Aspden et al., 1987; Cediel et al., 2003; Villagómez et al., 2011). This period initiated with syn-rift sedimentation (Cediel et al., 2003; Clavijo et al., 2008) and intrusion of Permian-

Triassic peraluminous granites (Vinasco et al., 2006; Cochrane et al., 2014), and culminated with the formation of a magmatic arc in the Late Triassic-Early Jurassic, represented by calc-alkaline I-type magmatism (Aspden et al., 1987; Clavijo et al., 2008; Cochrane et al., 2014). In the Aptian-Albian, the region transitioned to a transpressive regime reflecting tectonic reorganization of the Farallones and South American plates, which marked the onset of the current Northern Andean Orogeny (Cediel et al., 2003). This distinct orogenic event is characterized by a combination of protracted oblique subduction and accretion episodes of oceanic lithosphere against the western continental margin, which imprinted the positive topography to the cordillera, caused intrusion of Late Cretaceous syn-orogenic granites and built the present active volcanic arc (Restrepo and Toussaint, 1988; Cediel et al., 2003; Pindell et al., 2005).

The Mesozoic-Cenozoic evolution of the Northern Andes is proposed to follow a model of accreted lithotectonic blocks or terranes, which constitute geologic domains with common histories that accreted episodically to the continental margin from allochtonous to para-authoctonous positions relative to the Amazonian Craton (Etayo-Serna et al., 1986; Cediel et al., 2003; Restrepo and Toussaint, 2020). These terranes were sutured by nearly N-S-striking regional faults that partitioned Northern Andean stress mainly with lateral and inverse displacements (Feininger, 1970; Etayo-Serna; 1986; Ego et al., 1995). This occured, however, in asynchronous fashion resulting in individual blocks exhibiting differential morphotectonic evolutions (Restrepo-Moreno et al., 2019). One of these regional-scale structures is the Palestina Fault System, which represents the Mesozoic suture between two regional blocks that constitute the Central Cordillera, the Chibcha Terrane to the east and Tahamí Terrane to the west (sensu Restrepo and Toussaint, 2020), or Chicamocha and Cajamarca-Valdivia terranes (sensu Cediel et al., 2003) respectively. The northern termination of the Palestina Fault System in the San Lucas Range corresponds to the San Lucas Block (Etayo-Serna et al., 1986), a

transpressive pop-up structure (i.e., positive flower) with dextral kinematics whose evolution is affected by faults of the Palestina System such as Palestina, Otú, Nus, El Bagre and Cimitarra (Feininger, 1970; Barrero, 2000; García-Delgado and Velandia, 2020).

Amid this litho-structural mosaic are concentrated the most prolific gold deposits of the country along a metallogenic belt from Segovia-Remedios to Nechí towns (Ordóñez-Carmona et al., 2005; Sillitoe, 2008), that correspondingly display strong structural controls (Ordóñez-Carmona et al., 2005; González et al., 2010; Alvarez, 2013; Naranjo-Sierra et al., 2016). The most productive ore bodies are hosted by the Segovia Batholith, a granodioritic pluton that is part of an extensive Jurassic magmatic belt (~210-129 Ma) (Tschanz et al., 1974; Aspden et al., 1987; Leal-Mejía, 2011; Bustamante et al., 2016; Leal-Mejía et al., 2019). The Segovia Batholith was first described by Feininger et al. (1972) as "igneous rocks located mainly east of the Otú Fault" and adopted its name from its type locality, the Segovia municipality, where it intrudes the Proterozoic basement of the Central Cordillera eastern flank (Feininger et al., 1972; Álvarez, 1983; Gonzalez and Londoño, 2002) (FIGURE 1).

3. THE SEGOVIA-REMEDIOS MINING DISTRICT

The Segovia-Remedios Mining District is part of a 200 km-long Jurassic-Cretaceous metallogenic belt extended in the northernmost Central Cordillera (Sillitoe, 2008; Shaw et al., 2019). It includes the Lower Jurassic San Lucas Gold Province, the middle Jurassic Nechí District, and the Upper Cretaceous Zaragoza-Segovia-Remedios District, which comprise pluton-related, porphyry-related, hydrothermal, and epithermal type Au(Ag) occurrences hosted mainly in Jurassic plutonic and volcanic rocks (Shaw et al., 2019).

The Segovia Project of Gran Colombia Gold represents the southeastern portion of the Segovia metallogenic belt, covering an area of 3,000 ha in the municipality of Segovia, in the northeast Antioquia Department (FIGURE 1). The oldest geological unit in the zone is the 1.5 Ga-old San Lucas Gneiss (Cuadros, 2012), composed of quartz-feldspathic gneisses with interlayered

lenticular amphibolites and marble (Feininger et al., 1972). It is intruded by Permian anatectites and is in faulted contact with Triassic medium-grade metamorphic rocks of the Cajamarca Complex, located west of the Palestina Fault (Gómez et al., 2015). The Lower Jurassic Norosí Batholith and the Middle-Upper Jurassic Segovia Batholith intrude east of the Otú Fault (Feininger et al., 1972; Bogotá and Aluja, 1981), and are accompanied by coetaneous stocks (e.g. La Tinta), hypabyssal rocks, and unconformably-lying volcano-sedimentary strata (e.g. Noreán Formation) (Clavijo et al., 2008; Gómez et al., 2015). On the other hand, Lower Cretaceous gabbros, diorites, and granitic stocks (e.g. Santa Isabel), and the Upper Cretaceous Antioquia Batholith intrude west of the Otú Fault (Feininger et al., 1972). The youngest rocks are Paleogene-Miocene quartzdiorites and porphyries concentrated south of the Antioquia Batholith, and Pliocene volcano-sedimentary and sedimentary rocks located across the northern Otú Fault and east towards the Middle Magdalena Valley. (FIGURE 1).

Gold in the Segovia Project occurs in tabular quartz-sulfide veins ranging in thickness from a few centimeters to three meters (Echeverri, 2006) (FIGURE 2A). Ore mineralogy consists mainly of pyrite, sphalerite, and galena, with subordinate chalcopyrite, pyrrhotite, and electrum, whereas quartz and calcite are present as gangue minerals (Echeverri, 2006).

Veins formed following a three-stage paragenetic sequence represented by (i) large deposition of smoky and drusiform quartz with pyrite clots, and deposition of the first generation of sphalerite, galena, arsenopyrite and pyrrhotite (Alvarez, 2013). This was a pre-mineral barren stage (Manco et al., 2012), although minor Au could have precipitated at the end (Echeverri, 2006; Alvarez, 2013). (ii) Pyrite brecciation, quartz recrystallization, and precipitation of sphalerite, galena, and chalcopyrite in sulfide bands (Alvarez, 2013), plus a hydrothermal event with sericite+chlorite alteration (Manco et al., 2012). This stage represents the main mineralization event, which occurred in the Late Cretaceous as indicated by 88 to 81.3 Ma Ar-Ar and K-Ar ages in hydrothermal sericite (Leal-Mejía, 2011; López et al., 2018). (iii)

Formation of calcite veins cutting mineralization, accompanied by a weak, low volume hydrothermal event (Manco et al., 2012). This last stage was post-mineral and had no Au enrichment associated (Manco et al., 2012; Alvarez, 2013) (FIGURE 2B).

Mineralization in the Segovia Project deposited in three fracture sets secondary to the Otú Fault to form four main vein systems, El Silencio, Providencia, Cogote, and Las Verticales (Rusell, 1959; Echeverri, 2006). These structures were developed in-depth within the Segovia Batholith and filled during its exhumation (Rusell, 1959). However, current models propose that mineral fluids and heat derived from the Antioquia Batholith and were channeled through the Otú Fault during accretion of the Tahamí/Cajamarca-Valdivia Terrane (Echeverri, 2006; Echeverry et al., 2009; Álvarez, 2013). Furthermore, veins are in close association with dikes that are coetaneous to the Antioquia Batholith magmatism (Leal-Mejía, 2011), and are considered pre-mineral magmatic components that induced fluid precipitation and as likely metal source (Álvarez, 2013) (FIGURE 2D, 2E). Following mineralization, veins were displaced by vertical faults interpreted to reflect late Miocene deformation (SRK Consulting, 2018) (FIGURE 2F, 2G).

4. LOW-TEMPERATURE THERMOCHRONOLOGY IN ORE DEPOSITS

Geo-thermochronological methods use the nuclear decay of radioactive isotopes to date geological processes in rocks (White, 2013). Radiometric ages obtained from these methods are apparent ages interpreted as the time elapsed since a rock sample passed through a critical temperature (Reiners et al., 2015). This *closure temperature* (Dodson, 1973) varies for each mineral system covering a wide interval that allows reconstructing the thermal trajectory of a rock unit from its crystallization to its final exposure at the surface (Reiners et al., 2015; Restrepo-Moreno et al., 2019).

Low-temperature thermochronology encompasses the coolest range of mineral systems that are sensitive to temperatures equivalent to the upper crust (i.e. <300°C = <10km) thus recording

processes such as mineralization, hydrothermal activity, and cooling (Reiners et al., 2005; Bernet et al., 2019). Moreover, cooling can be translated into uplift, exhumation, and faulting using age-elevation relationships and geological constrains (Ehlers and Farley, 2003; Gallagher et al., 2005; Reiners et al., 2005; Foster, 2019). Some common geo and thermochronometers with their closure temperature intervals are displayed in FIGURE 3.

The Zircon Fission Track (ZFT) and Apatite Fission Track (AFT) methods are based on damage tracks left in the crystals when an unstable nuclide of ^{238}U decays by spontaneous fission (Reiners et al., 2005). These *fission tracks* are enlarged by chemical etching to be observable and counted under an optical microscope, which allows calculating the apparent closure-temperature age (Fleischer et al., 1965). However, if the sample reaches higher temperatures, the fission tracks begin to shorten by solid-state diffusion and yield younger ages which become eventually zero when fully annealed (Reiners et al., 2005). This means that fission tracks contain integrated information on thermal age and thermal hisotry given by track density and track length (Ketcham, 2005).

The (U-Th)/He dating system is based on the accumulation of He isotopes in zircon (ZHe) and apatite (AHe), derived from the α-decay of U and Th decay chains (Ehlers and Farley, 2003). Similar to the fission-track method, (U-Th)/He ages decrease with increasing temperature as He can diffuse out of the crystal, which acts as the effective diffusion domain thus be retained just partially (Wolf et al., 1998; Ehlers and Farley, 2003; Reiners, 2005).

In mining districts, these techniques provide a means to directly date ore formation and hydrothermal alteration by analyzing annealing/retention patterns in horizontal transects across veins and altered host rock (Bernet et al., 2019; e.g. Echeverri, 2006). Also, it is a powerful tool to reconstruct the thermal history of ore bodies by modelling the time-temperature history of unaltered host rock in vertical profiles (Bernet et al., 2019), which is essential to determine the timing and depth of host-rock intrusion, assess preservation potential in uplifted regions

(Kesler and Wilkinson, 2006; Bernet et al., 2019), and identify thermal anomalies related to more prospective areas (McInnes et al., 2005).

5. METHODOLOGY

This study used secondary sources of information (geochronology, geochemistry, structural geology) combined with fieldwork data and petrographic characterization to analyze the geological framework of the Segovia Batholith. The work focused on using low-temperature thermochronological data to reconstruct the thermal history for different tectonic-structural blocks at a local and regional scale, and the related mineralization.

5.1. Geological database

First, an extensive literature review of the Segovia Batholith was conducted and all to-date geological data was compiled. Second, El Silencio and Providencia mines of the Segovia Project were visited to recognize ore deposit characteristics. Gran Colombia Gold, company that operates the mining project, provided fourteen drill core samples of the Segovia Batholith, from which six were used to obtain samples for thin section analyses. Representative samples were selected considering the structural distribution of the cores within the project, and mineralogical and textural features observed in hand sample. Thin sections were prepared in Luis Felipe Peña Laboratory (Bogotá) and analyzed at EAFIT University (Medellín) using an Olympus petrographic microscope. Third, secondary and primary data were merged in a geodatabase, from which maps and graphics for each type of data were generated using ArcMap 10.5 software. Geochronology and petrography graphics were made in R software environment using ggplot2 and ggtern packages, respectively (Wickham, 2016; Hamilton and Ferry, 2018). Structural data was illustrated in Stereonet 10.4.6 (Cardozo and Allmendinger, 2013), and geochemistry plots were made using Petrograph 1.0.5 (Petrelli et al., 2005).

5.2. Thermal modeling

Thermochronological data generated in the northern Central Cordillera in previous studies was analyzed using a multi-dating and vertical profile approach, considering different regional tectonic blocks and local structural blocks. First, AFT and AHe ages were compiled, as these are the lowest-temperature thermochronometers thus better recording exhumation processes (FIGURE 3). Then, Age-Elevation Relationship (AER) profiles were constructed as a first approach to identify exhumation pulses and check for data consistency. The AER profiles were interpreted assuming that all samples crossed each isotherm at the same elevation; in this manner, ages of the same thermochronometer should be older towards the top of the profile, as they crossed the closure temperature isotherm earlier (Gallagher et al., 2005). To test interpretations derived from AER profiles, some samples were selected to construct time-Temperature (t-T) models for the regional and local structural blocks.

The samples to construct the models were selected looking for consistency and robustness based on four criteria. First, ages from higher-temperature systems must be successively older for each sample. Second, samples that the primary authors collected close to veins or interpreted as annealed were discarded. Third, samples with more ages from different systems were given preference. Fourth, samples located close to the mean age interval of each system were preferred. These criteria were considered sufficient to obtain representative time-temperature histories for a given tectonic-structural block with common evolution.

Exhumation rates were calculated from the t-T models with the ΔTemperature/ΔAge ratio using the closure temperatures of each system indicated in FIGURE 3, and a mean thermal gradient of 25 °C/km common for continental subduction zones (Gleadow and Brown, 1999).

Some uncertainties that arise from inferring exhumation histories from thermal trajectories include variable geothermal gradients in space and with time, topography, and local alteration of isotherms due to circulation of hot fluids or underground waters (Reiners et al., 2015). The

analysis presented here assumed ideal conditions with constant thermal gradient and no interaction with cold fluids; alteration from hydrothermal fluids is expected to be recorded by fission-track annealing, and effects of topography in the isotherms should be apparent in the AHe system. In this manner, constrains provided by multiple-dating are expected to surpass the uncertainty of the method.

6. RESULTS

6.1. Petrography

The Segovia batholith is in general a massive body, often ranging from slightly laminated to strongly gneissic close to the Otú fault zone where it presents local brecciated and millonitized zones (González, 2001; González et al., 2010). In addition, outcrops in road cuts are highly weathered (González and Londoño, 2002), and saprolite reaches 15 to 70 m thick in drill core samples.

Petrographic analysis and modal compositions of 18 samples are compiled here in the plutonic QAP classification diagram (after Streckeisen, 1976), 12 from previous work and 6 from the current (TABLE 1). As Feininger et al. (1972) noted when they first described the Segovia batholith, it is heterogeneous in composition and texture; although characterized by diorites and quartzdiorites, it presents gradational variations to more basic rocks such as hornblendic gabbros (González, 2001; Leal-Mejía, 2011). Consistently, samples here compiled classify from syeno-granite to diorite/gabbro and distribute seemingly random through the Segovia Project. Álvarez (2013) defined a lithological contact between quartzdiorites and granodiorites-tonalites towards the western limit of the project based on aerial expressions and petrography. However, the results presented and compiled here do not second this division (FIGURE 4).

In hand-sample scale, the Segovia Batholith present dominantly a phaneritic texture with coarse to medium grain-sized minerals. The grain size decreases close to shear zones as observed in

samples of the Providencia Mine, towards the southwestern limit of the study area, and increases locally to pegmatitic in various locations with K-feldspar grains as large as 2cm (FIGURE 5A, 5C). Textural and mineralogical variations are observed in the El Silencio Mine as gradational contacts between K-feldspar-rich pegmatitic rocks, to plagioclase-rich phaneritic facies (FIGURE 5D). In general, the samples show a color index between 10 and 30% and are composed mainly of plagioclase, quartz, potassium feldspar, biotite, and hornblende. Minor minerals observable in hand specimen include small pyrite grains which are disseminated in most samples, and secondary chlorite grains which are noticeable in pegmatitic samples.

Microscopically, samples show hypidiomorphic fabric and phaneritic texture, and pegmatitic samples are seen relatively porphyritic in thin section, with feldspar phenocrysts and occasional biotite glomerocrysts (FIGURE 6A, 6B). The major mineralogy remains as mentioned, with a significant presence of chlorite, sericite, biotite, saussurite, calcite and sulfides as secondary minerals, and minor presence of sphene, apatite, magnetite, and zircon as accessory minerals. Petrographic descriptions per sample are found in Appendix 1. Here, the most relevant alteration and textural features are summarized.

Chlorite appears as characteristic alteration product of biotite and often hornblende. It shows light-to-dark green color and low birrefringence with common blue or brown interference color. Complete pseudomorphs after biotite are often observed, yet partial alteration is more abundant. It is also observed in veinlets associated with calcite.

Sericite appears as fine mica aggregates replacing K-feldspar and plagioclase with preferential alteration localized in the core and along cleavage of the crystals. In porphyritic samples, altered phenocrysts as well as pervasive aggregates in the ‘matrix’ (i.e., medium-grained assemblages in pegmatitic samples) are observed. Furthermore, alteration rims are formed in biotite where in contact with plagioclase (FIGURE 6C).

Secondary biotite is recognized as aggregates of small green crystals (in PPL), which are distinguished from chlorite-altered grains by its third-order interference color. In samples with no strong deformation, transition from brown to pale and green-colored biotite is accompanied by carbonate alteration (FIGURE 6D).

Saussurite replaces plagioclase occuring as a distinct mixture of epidote, zoisite and sericite; epidote occurs as euhedral-to-subhedral prismatic crystals following the plagioclase cleavage, whereas zoisite occurs as smaller subhedral-to-anhedral crystals. Saussuritization is particularly strong in sample SE-06 located near Sandra K vein (FIGURE 4), where only plagioclase borders remain unaltered. In addition, where alteration to saussurite is far advanced, composite alteration assemblages are observed in pseudomorphs after biotite, with chlorite+epidote and chorite+epidote+carbonates (FIGURE 6E).

Exsolution textures include perthitic as lamellae of plagioclase in alkali-feldspar, graphic as intergrowths of alkali feldspar and quartz, and sagenitic as needlelike inclusions of rutile/sphene in biotite intersecting at 60°. Deformation textures include undulose extinction in quartz and the formation of narrow shear bands. The last is accompanied by quartz recrystallization, folding of pertite lamellae, formation of secondary green biotite, and fracturing of hornblende and plagioclase (sample SE-14, FIGURE 6F).

6.2. Structural geology

The Segovia Project is a gold-vein type deposit that displays a strong structural control by the Otú Fault in pre- syn- and post-mineral stages (Ordóñez-Carmona et al., 2005; Sánchez et al., 2007; Echeverry et al., 2009; Alvarez, 2013). Structural field data (TABLE 2) is integrated with compiled data from previous investigations to analyze the structural framework in the Segovia Project.

Three sets of fractures are interpreted to have formed in the Segovia Batholith during its emplacement. (i) a conjugate system oriented NE and NW with shallow and steep dike

intrusions associated, (ii) a “clean” fracture system (i.e. no dikes) striking NW with shallow dip, and (iii) a system oriented NNW with vertical dip (Rusell, 1959; Rodriguez and Pernet, 1983). This fracture set was sequentially filled with hydrothermal fluids as it developed to form the main vein systems of the Segovia Project (Sánchez et al., 2007).

In the pre-mineralization stage before the Upper Cretaceous, the first set of fractures formed the structures of the El Silencio System (Rusell, 1959), which comprises the El Silencio and Sandra K veins and strikes between 354-005 with average dip 40°E. Conjugate to El Silencio was formed the Cogote System comprising the Marmajito, Cogote, and Doña Ana veins (Rusell, 1959), which strike 293 to 340 and dip in average 40°E. The development of this set is associated with contraction forces during cooling of the Segovia Batholith or caused by intrusive-induced compression of the batholith itself. Such fracturing mechanisms are common in several plutons in Antioquia and are considered channels for mineral fluid ascend (Feininger et al., 1972). Considering El Silencio and Cogote fractures conjugate, NNW-oriented maximum shear stress is interpreted by Tremlet (1955).

In the syn-mineralization stage starting in the Upper Cretaceous (Leal-Mejía, 2011; López et al., 2018), mineral fluids precipitated in the first set of fractures to form the El Silencio and Cogote vein system, and a second fracture set was introduced and filled to conform the Providencia Vein System, which strikes 270-300, and dips approximately 40°E. Rusell (1959) argues it formed in a heterogeneous medium obstructing the development of conjugate fractures, although the NE fractures of the first set could have acted as conjugate (Rodriguez and Pernet, 1983). Echeverri (2006) interpreted Providencia as contemporaneous to El Silencio, and Echeverry et al. (2009) assign a younger age based on cutting relationships, although they report ‘Providencia’ as a 070-striking/50°E-dipping structure, which does not match the character of the system. Here, Providencia is regarded as precipitated after El

Silencio, following the original chronology of the fracture sets by Rusell (1959); even though he did not name this system, his second fracture set is concordant with Providencia.

The calculated mean strikes of the Silencio, Cogote, and Providencia vein systems are 020, 320, and 290, respectively (FIGURE 7). Considering the symmetry between these systems and their relation to stress fields (Anderson, 1951), it is suggested that they represent secondary (R', R, P) structures of a main fault (Y) striking 305 with dextral imposed shear. The current 320 strike of the Otú Fault at the latitude of the Segovia Project, permit to establish it as the main fault controlling the development of mineral fracture-veins. The angle gap between theorical and real-mean strikes can be explained by an oscilating NW- to NNE-oriented compression, as also proposed by Tremlett (1955) for the conjugate El Silencio-Cogote sets; or might be a result of the Otú Fault inflection in the study area, compared to the 350-striking fault trace immediately north and south of the Segovia Project. In El Silencio Mine, t-fractures trending 310-320 indicate a NW-SE compressional stress tensor (FIGURE 2C); whereas NNE-oriented compression interludes might relate to stress dissipation and partition in horsetail structures, as characteristic in the El Silencio Vein (SRK Consulting, 2018). Furthermore, this chronology corresponds to emplacement of the Segovia Batholith at ~240°C (~10 km) based on ZFT data (Echeverri, 2006). Accordingly, en-echelon tension fractures indicate deformation in the ductile-fragile transition regime.

In the post-mineralization stage the Las Verticales System formed, which dips nearly vertical and strikes between 315 and 350, parallel to the Otú Fault trace in this area. It is restricted to the western limit of the Segovia Project, identified in the Cecilia and Tres y Media mines (Rusell, 1959). It represents a shear zone interpreted to reflect WNW-oriented late Miocene deformation that displaces veins such as Providencia (SRK Consulting, 2018). Under this stress tensor, new ENE-oriented faults are formed in the northern area of the project (e.g. K Fault). Altogether, post-mineralization deformation accounts for vertical displacement of the veins by

>50m (SRK Consulting, 2018) in a fragile structural regime, as suggested by strong fracturing (Echeverry et al., 2009) and development of fault-gouge bands in the El Silencio Mine (FIGURE 2G).

According to this structural framework, two structural blocks are defined in the Segovia Project named according to the vein system they enclose, the Silencio block located northeast between the K Fault to the north and the Cogote System to the south, and the Providencia block located southwest from the Cogote System through the southern limit of the project (FIGURE 7).

6.3. Cooling history of the Segovia Batholith

Based on the tectonic framework, two lithotectonic blocks define the study area at a regional scale, here called the Central Cordillera Block to the west of the Otú Fault, and the San Lucas Block to the east. Geo-thermochronological data of the former is compiled from Saenz (2003), Restrepo (2009), Leal-Mejía (2011), and Villagómez and Spikings (2013); and data of the latter is compiled from Echeverri (2006), Caballero et al. (2013), and Noriega-Londoño (in review). The spatial distribution of the samples is presented in FIGURE 8, and the temporal distribution is displayed in AER profiles (FIGURE 9, 10).

In the Central Cordillera Block, data derives predominantly from the Antioquia Batholith, located centrally in the block. U-Pb data yields three age groups of ~94Ma, ~88-84 Ma, and ~75-71 Ma, which correspond to syn-collisional magmatic pulses of the Antioquia Batholith (Duque-Trujillo et al., 2019). Thermochronometers are arranged in three intervals as follows. Cooling between 500 and 300°C is registered by K-Ar ages in biotite of ~81-71 Ma, and Ar-Ar ages in various systems between ~80 and ~63 Ma. In this interval also fall some ZFT and AFT outlying samples. Altogether, it is interpreted to reflect Late Cretaceous-early Paleocene cooling. The next cooling interval between 240°C and 110°C is marked by ZFT ages concentrated at ~58-46 Ma, AFT ages ranging from ~58 to ~38 Ma, a single ZHe age yielding 45.5 Ma, and a first older population of AHe ages from ~49 to ~43 Ma. These ages are dispersed

in a continuous interval from ~58 to ~38 Ma, representing a late Paleocene to Eocene cooling event. Last, a younger population of AHe ages yield ~34 to ~20 Ma, which corresponds to a third cooling event in the Oligocene (FIGURE 9).

In the San Lucas Block, compiled samples correspond to the San Lucas Gneiss, the Ité Granite, and the Norosí and Segovia batholiths, distributed through the entire block. U-Pb ages define two clusters at ~185 Ma and 159 Ma, consistent with crystallization ages of the Norosí and Segovia batholiths, respectively. ZFT ages are arranged in two groups at ~83 and ~65 Ma, and AFT ages range from ~65 to ~51 Ma, representing cooling between 240 and 110 °C in the Late Cretaceous to early Eocene. Next, ZHe ages yield ~74 to ~45 Ma, and AHe ages are dispersed between ~48 and ~17 Ma but clustered around 34 Ma. They represent a continuous cooling period from Eocene to Miocene (FIGURE 10). Worthy of mention is the negative trend in the AER profile of this block, with ages becoming younger with altitude, as opposed to the expected tendency. Having a spaced sampling transect versus a shallow topographic profile is likely causing the slope inversion, thus exhumation rates should not be calculated from it (Peyton and Carrapa, 2013).

A comparison of the age-elevation distribution between the two regional blocks at the latitude of Segovia, shows different age intervals at similar elevations, suggesting they have cooled asynchronously (FIGURE 11).

Mean exhumation rates per block were calculated assuming a geothermal gradient of 25°C/km. Data in the Central Cordillera Block is highly dispersed, thus the mean was calculated using only the most frequent data interval to reduce the effect of samples with outlying, unlikely exhumation rates (e.g. 6.50 km/My). In contrast, data in the San Lucas Block is less variable hence the means were calculated for all the samples.

The calculated mean exhumation rates for the Central Cordillera Block are 0.50 km/My between the ZFT-AFT systems and 0.16 km/My between the AFT-AHe systems (FIGURE

12A, 12B). In the San Lucas Block are obtained mean exhumation rates of 0.28 km/My between the ZFT and AFT systems, and 0.20 km/My between the ZHe and AHe systems (FIGURE 12C, 12D).

Using the samples with coherent exhumation rates, time-temperature (t-T) trajectories were constructed for each block. The t-T path for the Central Cordillera Block shows a segmented curve with the steeper slopes marking exhumation pulses. Concordant with the pattern observed in AER profiles, the t-T path pinpoints two exhumation events in the Late Cretaceous and Paleocene-Eocene. The Oligocene cooling episode identified in the AER profile, however, is not evident in the t-T path (FIGURE 13). Exhumation rates recalculated for these two segments as the slope between breakpoints correspond to 1.47 km/My for the Late Cretaceous event and 0.41 km/My for the Paleocene-Eocene episode. The former may be an overestimation as the Antioquia Batholith was cooling from both post-magmatic relaxation and exhumation and is not possible to discern between the two. However, post-magmatic cooling of intrusions emplaced in the middle-lower crust may not be recorded by low-temperature thermochronometers (Bernet et al., 2019), and similar rates of 1.6 km/My are obtained for a 75-70 Ma exhumation pulse identified in previous thermochronological models (Villagómez and Spikings, 2013).

In the San Lucas Block, a less segmented t-T path is apparent, with a continuous, slow cooling trend from the Jurassic to the Late Cretaceous. Then, an inflection point at ~84 Ma marks the onset of a Late Cretaceous to early Eocene exhumation event at rates 0.16 km/My, followed by a shallower trend in the Eocene-Miocene (FIGURE 14).

7. DISCUSSION

7.1. Spatial distribution and tectonomagmatic setting

The Segovia Batholith is bounded by the Otú Fault to the west and the Palestina Fault to the east. Current U-Pb and K-Ar ages indicate a Middle Jurassic to Lower Cretaceous crystallization age from ~165 to ~140 Ma (Feininger et al., 1972; Leal-Mejía, 2011; Álvarez, 2013; López et al., 2018), product of an apparently continuous magmatism. Older U-Pb crystallization ages dating around 185 Ma (e.g., 188.9 ± 2 Ma by Cochrane et al., 2014) correspond to the Norosí Batholith, located east of the Palestina Fault (Bogotá and Aluja, 1981; Leal-Mejía et al., 2019). This unit is distinguished from the Segovia Batholith by a higher cortical component indicated by more negative εNd(T) values and initial $^{87}Sr/^{86}Sr$ ratios greater than 0.7045 (Cuadros, 2012). On the other hand, a Late Cretaceous U-Pb age obtained in El Silencio Mine (81.9 ± 6.6 Ma by López et al., 2018) is not considered representative to suggest a younger magmatic pulse of the Segovia Batholith as the authors propose (López et al., 2018). Samples located in the central part of the batholith near the Segovia Project have younger ages, whereas the oldest samples are located towards the northern and southern limits of the batholith, with no apparent latitudinal distribution pattern. On the other hand, the longitude vs. age diagram shows that samples tend to be younger to the west (FIGURE 15). The latter trend reflects at a unit-wide scale the regional west-younging trend observed in northern Jurassic batholiths in an E-W transect Santander Plutonic Group – San Lucas Granitoids (including the Norosí Batholith) – Segovia Batholith (Leal-Mejía et al., 2019).

Compiled lithogeochemical data of the Segovia Batholith show intermediate to acid composition of the calc-alkaline to high-K calc-alkaline series (FIGURE 16A, 16B). Multi-element diagrams display typical trends for subduction-related magmas (FIGURE 16C, 16D), and tectonic discrimination diagrams display volcanic-arc affinity (FIGURE 16E). Moreover, it shows a mantellic isotopic signature with εNd(t) between -2.7 and +6.7, and $^{87}Sr/^{86}Sr_{(i)}$ ratios

<0.704 (Ordóñez-Carmona et al., 2005; Leal-Mejía, 2011; Álvarez, 2013; FIGURE 16F). These geochemical characteristics suggest relation with an extensional subduction setting and are concordant with the formation of a transtentional basin in the San Lucas Range in the Triassic-Jurassic (Sarmiento et al., 2006; Clavijo et al., 2008). Extension may be driven by rifting associated to the opening of the Proto-Caribbean basin to the north (Cediel et al., 2003), or it may be driven by slab rollback of the Pacific Plate to the west (Cochrane et al., 2014; Spikings et al., 2015). The contemporaneity of these major tectonic events complicates the definition of a unique setting (Clavijo et al., 2008; Bayona et al., 2020). Another hypothesis to explain the more juvenile character of the Segovia Batholith is the presence of a continental float between the Otú and Palestina faults (Leal-Mejía et al., 2019). Considering the structural reconstruction of these faults by Feininger et al. (1972), it is apparent that before left-lateral movement of the Otú Fault in the middle Cretaceous, the Norosí and Segovia batholiths were located in a southern position, separated by the paleo-Palestina Fault. In this scenario, the narrow southern portion of the Segovia Batholith between the Palestina and Nus-Bagre faults would correspond to the Norosí Batholith. This would further explain the older ages and more cortical isotopic character registered in samples located in this segment, near the Monte Cristo Quarry (εNd(t) value of -7.18). In this sense, the first crystallization age of the Segovia Batholith obtained in this location by Feininger et al. (1972) using K-Ar, would actually correspond to the Norosí Batholith and represent a different magmatic episode separated by the Palestina Fault.

7.2. Lithological character

Studies advanced in the Segovia-Remedios Mining District attempted to divide the Segovia Batholith into magmatic-isotopic pulses (Ordóñez-Carmona et al., 2005) and lithological facies in the Segovia Project (Álvarez, 2013), yet compiled geochronological, geochemical, and petrographic data presented here remain scattered. No systematic variations are recognized that

allow discriminating pulses or facies of the Segovia Batholith, and analyze the possible controls that variations of these features would exert in the mineralization.

In the Segovia Project, the Segovia Batholith is classified from syeno-granite to diorite/gabbro with a predominance of granodiorites based on modal analyses. Hydrothermal alteration assemblages analyzed in this study correspond to propylitic alteration with chlorite+epidote+calcite, and sericitization with sericite+quartz+sulphides, being especially strong in sample SE-08 collected between the El Silencio and Sandra K mines. This configuration is interpreted to represent a hydrothermal alteration event localized in the NE area of the Segovia Project, probably at a temperature of ~340°C, as indicated by Álvarez (2013) using the chlorite thermochronometer in samples of the El Silencio Mine. On the other hand, a local grain-size decrease and formation of shear bands in samples of the Providencia Mine in the southwestern limit of the Segovia Project is associated with proximity to the Las Verticales shear zone. Deformation textures such as undulose extinction in quartz indicate a temperature range of 300-400°C for this event (Passchier and Trouw, 1996).

7.3. Cooling history and exhumation

The cooling history constructed at a regional scale for the San Lucas Block registers three cooling stages for the Segovia Batholith. The first, from its crystallization in the middle-upper Jurassic to the Late Cretaceous, shows slow and continuous cooling typical of post-magmatic heat loss. An inflection point at ~84 Ma marks the start of an exhumation event at rates 0.16 km/My that extended until the late Paleocene; followed by a slow cooling period from Eocene to at least middle Miocene times. In contrast with previous thermal reconstructions interpreting evolution in a “tectonically-undisturbed quiescent environment” (Echeverri, 2006), here it is argued that the Segovia Batholith was responsive to episodes of increased uplift-exhumation that characterize the Late Cretaceous-Cenozoic evolution of the Central Cordillera (Saenz, 2003; Restrepo-Moreno, 2009; Spikings et al., 2015; Restrepo-Moreno et al., 2019).

The Late Cretaceous exhumation event interpreted here is also recorded in adjacent units of the Central Cordillera using multiple thermochronometers (Villagómez et al., 2013; Villagómez and Spikings, 2013), and in the eastern San Lucas Range with ZFT and AFT dating (Amaya et al., 2019), suggesting it corresponds to tectonic-driven early uplift of the proto-Central Cordillera (Villagómez et al., 2011). This exhumation-uplift event relates to the onset of oblique subduction of the Farallones Plate since the Aptian-Albian (Cediel et al., 2013) and strike-slip convergence of the Caribbean Plate since the Albian (Kennan and Pindell, 2009), which probably initiated exhumation ~84 Ma. Continuing in the latest Cretaceous, exhumation coincides with more directed convergence between the Caribbean and South American plates (Kennan and Pindell, 2009), added to the Caribbean LIP collision at ~75 Ma (Villagómez et al., 2011; Cochrane et al., 2014), and the final docking of the Tahamí Terrane (Restrepo and Toussaint, 2020). These successive crust-shortening events which influenced depositional patterns in Colombian basins, were named by Van der Hammen (1961) as Laramic orogenic phase, which was likely characterized by sustained exhumation through the Paleocene. Following exhumation, the Segovia Batholith experienced a period of diminished cooling from the Eocene to middle Miocene, apparently registering no exhumation driven by the pre-Andean orogenic episode (FIGURE 17).

7.4. Implications on mineralization in the Segovia Mining District

Mineralization in the Segovia-Remedios District is a result of tectono-magmatic, structural, and thermal processes, where accretion-subduction tectonics, host-rock deformation, regional faults kinematic, syn-collisional magmatism, and crustal thermal gradients all play a role. Each factor represents a complex process that could be further studied in detail. Here, it is called upon attention the concurrence in space and time of these processes and how linked they are with ore timing, distribution, and endowment (FIGURE 17).

The majority of preceding studies in the region emphasize the structural controls of the Otú Fault zone in mineralization, where the primary structure transport mineral fluids and second-order fractures receive them (Rusell, 1959; Ordóñez-Carmona et al., 2005; Sánchez et al., 2007; Echeverry et al., 2009; Alvarez, 2013). The source of such fluids remains unknown, as previous fluid inclusion analyses show physicochemical characteristics suitable for a wide range of metamorphic, igneous, and mantellic reservoirs (Manco et al., 2012; Álvarez, 2013). Notwithstanding, the strongest candidate is the Antioquia Batholith since it is contemporaneous with and spatially close to veins (Echeverri, 2006; Manco et al., 2012; Shaw et al., 2019). Álvarez (2013) assumes a lithospheric-mantle source following the theoretical models of Hronsky et al. (2012) for gold genesis in accretionary tectonic settings. This study argues that an enriched deep fluid source is not necessary, and supports fluid provenance from the Antioquia Batholith, which is a fertile source for numerous Cretaceous deposits (Shaw et al., 2019). Interestingly, the main mineralization phase at ~85 Ma (Leal-Mejía, 2011; López et al., 2018) and the hydrothermal alteration event at ~48 Ma (Echeverri, 2006) are coetaneous with the Late Cretaceous and Eocene exhumation pulses interpreted for the Antioquia Batholith (FIGURE 17). This suggests that fluid migration was synchronous with phases of increased tectonic shortening that affected the Antioquia Batholith at a crustal level.

Significantly lower exhumation rates in the San Lucas Block are interpreted to reflect the more distal position from the western deformation front, whereas the Central Cordillera Block exhumes faster. This scenario is analogous to normal-faulted blocks in which isotherm deflection in the hangingwall favors the conduction of hot fluids towards it (Ehlers et al., 2001). Under such scenario, thermal subsidence in the San Lucas Block may explain preferential fluid conduction from the rapidly uplifting Antioquia Batholith to the cooler Segovia Batholith through the Otú Fault acting as a permeable channel. Moreover, periodic magmatic pulses of the Antioquia Batholith from 97 to 58 Ma (Duque-Trujillo et al., 2018; Leal-Mejía et al., 2019),

combined with orogenic periods can trigger fluid expulsion and remobilization. The episodic nature of tectonic and magmatic events is reflected in the multi-stage character of the mineral paragenetic sequence (Echeverri, 2006; Manco et al., 2010; Álvarez, 2013), and the sequential filling of fracture-vein networks (Rusell, 1959; Sánchez et al., 2007; Echeverry et al., 2009).

7.5. Implications on ore grade in the Segovia Project

ZFT data collected by Echeverri (2006) is analyzed here considering the defined structural blocks, El Silencio and Providencia. In the northeastern El Silencio Block, ZFT ages yield 82.7 and 84.1 Ma, whereas in the southwestern Providencia Block, ZFT ages yield 68.4 and 62.1 Ma. Keeping in mind the K-Ar and Ar-Ar ages in sericite that constrain the timing of mineralization between ~88 and ~82 Ma (Leal-Mejía, 2011; López et al., 2018), a greater thermal gradient in the El Silencio block is evident (FIGURE 18). Variations in the thermal gradient might be indicating local deflection of the isotherms, with the higher thermal gradients in the El Silencio Block signaling the presence of a shallow heat source in the northeastern area of the project, where samples also show more intense alteration assemblages. The thermal gradient of the upper crust have important implications in metal and heat transfer, as the areas with higher thermal gradient transport metals more effectively and result in higher ore grades (McInnes et al., 2015). This being the case, differential thermal gradients per structural block would play an important control in ore endowment in the Segovia Project.

Measured and indicated grades for the El Silencio Vein are 10.3 g/ton, whereas Providencia has higher grades of 15.8 g/ton (SRK Consulting, 2018). Thus, structural controls as proximity to the transport corridor and metal source, here regarded as the Otú Fault and Antioquia Batholith, seem to be the first-order controls on ore endowment in the Segovia Project. Notwithstanding, the marked thermal gradient difference observed in local structural blocks might represent an additional control in gold precipitation, but the interpretation of these local variations on the isotherms is limited by scarce thermochronological data.

In comparison to other deposits in the Segovia-Remedios Mining District (Londoño et al., 2009; Castaño-Dávila et al., 2019), the veins in the Segovia Project are arranged at more complex geometries that differ from the theoretical secondary fractures of a main shear imposed by the Otú Fault. This is probably an effect of the westward inflection of the fault trace by >20° at the latitude of Segovia. As the structural configuration becomes less ideal, crustal thermal variations can become relevant and should be constrained to better target prospective exploration sites.

8. CONCLUDING REMARKS

- Compiled geochronological and geochemical data in the Segovia Batholith is distributed randomly. No magmatic pulses are distingishable.
- The Segovia Batholith in the Segovia Project is dominated by granodiorites with felsic and mafic variations to syeno-granites and diorites/gabbros. No petrographic facies are recognized with the sample density presented here; lithological distribution seems arbitrary and does not support previous petrographic contacts (e.g. Álvarez, 2013).
- The northeastern area of the Segovia Project is characterized by propylitic alteration assemblages between the El Silencio and Sandra K mines, whereas deformation textures dominate towards the southwestern limit of the project in the Providencia Mine next to the Las Verticales shear zone.
- An inflection point at ~84 Ma in the T-t curve of the San Lucas Block suggests a Late Cretaceous to Paleocene exhumation event at rates ~0.16 km/My, corresponding to early uplift of the proto-Central Cordillera related to oblique subduction of the Farallones Plate and collision of the Caribbean plateau.

- Asynchronous cooling and differential exhumation between the Central Cordillera and San Lucas blocks favors hydrothermal fluid conduction from the rapidly exhuming Antioquia Batholith to the cooler Segovia Batholith, channeled through the Otú Fault.
- Mineralization in the Segovia-Remedios Mining District results from regional coupled processes, such as shortening episodes of the Northern Andean Orogeny in the Late Cretaceous and Eocene, synorogenic magmatic pulses of the Antioquia Batholith in the Late Cretaceous-Paleocene, and activation of the Otú Fault in the middle Cretaceous.
- Mineralization in the Segovia Project is locally controlled by structural and thermal factors. Deformation along the Otú Fault zone imprints a first-order control in fluid channeling and host-rock deformation, and local variation of the isotherms may focus richer fluids in areas of increased thermal gradient.

9. RECOMMENDATIONS

Acknowledging ongoing petrological and geochemical characterization conducted by the company, the integration of additional techniques such as thermochronology is recommended as a proxy to possible thermal controls stressed here. Robust sampling in different structural blocks of the project, following both horizontal and vertical transects can help address various incognita: (i) the location of more areas with high thermal gradients, (ii) the extension of the hydrothermal system by testing or refuting the Eocene hydrothermal event dated previously by AFT but with no track-length measurements, (ii) the slip rates of thrust faults that displace mineralization, (iii) the preservation potential of underexplored areas, particularly to the north of the K Fault where veins from El Silencio System ‘disappear’, are they undeveloped in depth or exhumed? Moreover, future thermochronological studies should take advantage of track-length measurements to construct models using statistical software such as HeFTy.

10. REFERENCES

Alcárcel, F.A., Gómez, J (comp.). (2019). Mapa Geológico de Colombia 2019. Escala 1:2 000 000. Servicio Geológico Colombiano. Bogotá.

Álvarez, M., Ordóñez-Carmona, O., Valencia, M., Romero, A. (2007). Geología de la zona de influencia de la falla Otú en el distrito minero Segovia-Remedios. Revista DYNA 153, 41-51.

Alvarez A., J. (1983). Geología de la Cordillera Central y el occidente colombiano y petroquímica de los intrusivos granitoides mesocenozoícos. Boletín Geológico, 26(2), 175.

Álvarez, M. (2013). Petrologia, geoquímica isotópica e metalogenia dos depósitos de ouro El Silencio e La Gran Colombia, Distrito Mineiro Segovia-Remedios, Colombia. Master thesis, Universidade de Brasilia, Brasil.

Allmendinger, R. W., Cardozo, N. C., Fisher, D. (2013). Structural Geology Algorithms: Vectors & Tensors: Cambridge, England, Cambridge University Press, 289 pp.

Amaya, S., Bernet, M., Zuluaga, C.A., Villamizar, N., Urueña, C., Peña, M.L. (2019). Evolucion tectonotermal del flanco oriental de la Serrania de San Lucas. XVII Congreso Colombiano de Geología, Santa Marta, Colombia.

Anderson (1905). Facsimile reproduction of The Dynamics of Faulting by E. M. Anderson. Geological Society, London, Special Publications, 367, 231-246, 2012.

Aspden, J.A., McCourt, W.J., Brook, M. (1987). Geometrical control of subduction-related magmatism: the Mesozoic and Cenozoic plutonic history of Western Colombia. Journal of the Geological Society 144, 893-905.

Bayona, G., Bustamante, C., Nova, G., Salazar-Franco, A. (2020). Jurassic evolution of the northwestern corner of Gondwana: Present knowledge and future challenges in studying Colombian Jurassic rocks. The Geology of Colombia, 2 Mesozoic(April), 37. https://doi.org/https://doi.org/10.32685/pub.esp.36.2019.05

Bernet, M., Piraquive, A., Urueña, C., López-Isaza, J. A., Bermúdez, M. A., Zuluaga, C., Amaya, S., Villamizar, N. (2019). Multidisciplinary petro-geo-thermochronological approach to ore deposit exploration. Ore Geology Reviews, 112(July 2018), 103017. https://doi.org/10.1016/j.oregeorev.2019.103017

Bogotá, J., Aluja, J. (1981). Geología de la Serranía de San Lucas. Geología Norandina, 4.

Boynton, W.V. (1984). Cosmochemistry of the rare earth elements; meteorite studies. In: Rare earth element geochemistry. Henderson, P. (Editors), Elsevier Sci. Publ. Co., Amsterdam. 63-114.

Bustamante, C., Archanjo, C., Cardona, A., Vervoort, J. (2016). Late Jurassic to Early Cretaceous plutonism in the Colombian Andes: A record of long-term arc maturity. Sao Paulo: The geological society of America.

Caballero, V., Parra, M., Mora, A. (2013). Factors controlling selective abandonment and reactivation in thick-skin orogens: A case study in the Magdalena Valley, Colombia. Geological Society, London, Special Publications, 377, 343-367.

Castaño-Dávila, D. L., Hernández, J. S., Molano, J. C., Rodríguez, A. I. (2019). Mineralogía y microtermometría de inclusiones fluidas de la veta con mineralización Au-Ag de la mina

La Aurora en la parte norte del Distrito Minero Zaragoza–Segovia–Remedios (DMZSR), Colombia. Revista Boletín de Geología, 41(3), 107–125. https://doi.org/10.18273/revbol.v41n3-2019005

Cediel, F., Shaw, R., Cáceres, C. (2003). Tectonic assembly of the Northern Andean Block, in Bartolini, C. et al. The Circum-Gulf of Mexico and the Caribbean: Hidrocarbon, habitats, basin formation, and plate tectonics. AAPG memoir, 79, 815-848.

Clavijo, J., Mantilla, L., Pinto, J., Bernal, L., Pérez, A. (2008). Evolución geológica de la serranía de san lucas, norte del valle medio del magdalena y noroeste de la cordillera oriental. Boletin de Geología, 30, 45-62.

Cochrane, R., Spikings, R., Gerdes, A., Winkler, W., Ulianov, A., Mora, A., Chiaradia, M. (2014). Distinguishing between in-situ and accretionary growth of continents along active margins. Lithos, 202–203, 382–394.

Collins, D. E., Belalcázar, G., Page, W. (1981). Quaternary activity of the Palestina Fault zone NW de Colombia. Revista CIAF, 6 (1 – 3), 1-17.

Cordani, U., Cardona, A., Jimenez, D., Liu, D., Nutman, A. (2005). Geochronology of Proterozoic basement inliers in the Colombian Andes: Tectonic history of remnants of a fragmented Grenville belt. Geological Society Special Publication, 246, 329–346.

Cox, K.G., Bell, J., Panhurts, R. (1979). Trace elements in igneous processes. In: The Interpretation of Igneous Rocks. Dordrecht: Springer

Cuadros, F (2012). Caracterizacao geoquimica e geocronologica do embasamento Mesoproterozoico da parte norte da Serrania de San Lucas (Colombia). Master thesis, Universidade de Brasilia, Brasil.

Dodson, M.H. (1973). Closure temperature in cooling geochronological and petrological systems. Contributions to Mineralogy and Petrology, 40, 259–274. https://doi.org/10.1007/BF00373790

Duque-Trujillo, J., Bustamante, C., Solari, L., Gómez-Mafla, A., Toro-Villegas, G., Hoyos, S. (2019). Reviewing the Antioquia batholith and satellite bodies: a record of Late Cretaceous to Eocene syn-to post-collisional arc magmatism in the Central Cordillera of Colombia: Andean Geology, 46(1) p. 82-101.

Echeverri, B. (2006). Genesis and thermal history of gold mineralization in the Segovia-Remedios Mining District of Northern Colombia. Master thesis, Shimane University, Japan.

Echeverry, S., Cárdenas, A., Ordóñez-Carmona, O., Muñoz Aguare, O. (2009). Aspectos estructurales y relaciones de algunos sistemas vetifomes del distrito minero Segovia-Remedios. Boletín Ciencias de La Tierra, 26, 1–9.

Ego, F., Sébrier, M., Yepes, H. (1995). Is the Cauca-Patia and Romeral Fault System left or rightlateral? Geophysical Research Letters, 22(1), 33–36. https://doi.org/10.1029/94GL02837

Ehlers, T. A., Farley, K. A. (2003). Apatite (U-Th)/He thermochronometry: Methods and applications to problems in tectonic and surface processes. Earth and Planetary Science Letters, 206(1–2), 1–14.

Etayo-Serna, F., Barrero, D., Lozano, (1986). Mapa de terrenos geológicos de Colombia. INGEOMINAS. Publicaciones Geológicas Especiales del INGEOMINAS, 14(1), 1–135.

Feininger, T., Barrero L., D., Castro Q. (1972). Geologia de parte de los departamentos de Antioquia y Caldas (sub-zona II-B). Boletín Geológico, 20(2), 173.

Fleischer, R. L., Price, P. B., Walker, R. M., Leakey, L. S. B. (1965). Fission Track dating of bed I. Olduvai Gorge: Science, Vol. 148, p. 72-74.

Gallagher, K., Stephenson, J., Brown, R., Holmes, C., Fitzgerald, P. (2005). Low temperature thermochronology and modeling strategies for multiple samples 1: Vertical profiles. Earth and Planetary Science Letters, 237(1–2), 193–208.

García-Delgado, H., Velandia, F. (2020). Tectonic geomorphology of the Serranía de San Lucas (Central Cordillera): Regional implications for active tectonics and drainage rearrangement in the Northern Andes. Geomorphology, 349, 106914.

Gleadow, A., Brown, R. (1999). Fission track thermochronology and the long-term denudational response to tectonics. In Summerfield, M.A. (Ed.), Geomorphology and Global Tectonics, (pp. 57-75). Chichester, England: John Wiley and Sons Ltd.

Gómez, J., Montes, N.E., Nivia, Á., Diederix, H., compilers (2015). Geological Map of Colombia 2015. Scale 1:1 000 000. Servicio Geológico Colombiano. Bogotá.

González, H., Londoño, A. (2002). Catálogo de las unidades litoestratigraficas de Colombia: Diorita de Segovia. INGEOMINAS, Bogotá. 19 pp.

González, J., Terán, B., Ordóñez-Carmona, O. (2010). Geología de la parte oriental del distrito minero Segovia - Remedios. Boletín de Ciencias de La Tierra, 28, 61–76.

Hamilton N.E., Ferry, M. (2018). "ggtern: Ternary Diagrams Using ggplot2." Journal of Statistical Software, Code Snippets, 87(3), 1–17. doi: 10.18637/jss.v087.c03.

Irving, E. (1975). Structural Evolution of the Northernmost Andes , Colombia Structural Evolution of the Northernmost Andes , Colombia. Geological Survey Professional, 846.

Kennan, L., Pindell, J. (2009). Dextral shear, terrane accretion and basin formation in the Northern Andes: best explained by interaction with a Pacific-derived Caribbean Plate?. In The origin and evolution of the Caribbean plate. Geological Society of London Special Publications, 328, 487- 531.

Kerr, A., Marriner, G., Tarney, J., Nivia, A., Saunders, A., Thirlwall, M., Sinton, C. (1997). Cretaceous basaltic terranes in Western Colombia: Elemental, chronological and Sr-Nd isotopic constraints on petrogenesis. Journal of Petrology, 38(6), 677–702. https://doi.org/10.1093/petroj/38.6.677

Kesler, S.E., Wilkinson, B.H. (2006). The role of exhumation in the temporal distribution of ore deposits. Economic Geology 101, 919–922.

Ketcham, R. (2005). Forward and inverse modeling of low-temperature thermochronometry data. Reviews in Mineralogy and Geochemistry, 58(May), 275–314. https://doi.org/10.2138/rmg.2005.58.11

Leal-Mejía, H. (2011). Phanerozoic gold metallogeny in the Colombian Andes: a tectonomagmatic approach. Doctoral thesis, Universitat de Barcelona, Spain.

Leal-Mejía, H., Shaw, R., Melgarejo, J. (2019). Spatial-Temporal Migration of Granitoid Magmatism and the Phanerozoic Tectono-Magmatic Evolution of the Colombian Andes. In: Cediel, F., Shaw, P (Eds.). Geology and Tectonics of Northwestern South America. (pp. 253-410). Frontiers in Earth Sciences.

López, J., Luengas, C., Velásquez, L., Celada, C., Sepúlveda, M., Prieto, D., Gómez, M.

(2018). Memoria explicativa mapa metalogénico de Colombia: principios, conceptos y modelos de depósitos y manifestaciones u ocurrencias minerales para Colombia. Servicio Geológico Colombiano, Bogotá. 189 pp.

Manco, J., Molano M., J., Ordoñez-Carmona, O. (2012). Paragenetic and microthermometric analysis of the Au-Ag ores from the Segovia-Remedios Mining Distric (SRMD): Implications for the source and nature of the ore-forming fluids. Boletín de Ciencias de La Tierra, 32, 47–60.

Maya, M., González, H. (1995). Unidades litodemicas en la Cordillera Central de Colombia. Boletín Geológico, 35(March), 43–57.

McInnes, B., Evans, N., Fu, F., Garwin, S. (2005). Application of thermochronology to hydrothermal ore deposits. Reviews in Mineralogy and Geochemistry, 58, 467–498. https://doi.org/10.2138/rmg.2005.58.18

Naranjo-Sierra, E., Zapata, E., Alvaran, M. (2016). Análisis metalogenético preliminar del depósito vetiforme en la mina La Ye , Antoquia , Colombia : características geológicas, isotópicas y estructurales. Revista Mexicana de Ciencias Geológicas, 33 (3), 316–328.

Nakamura, N. (1974). Determination of REE, Ba, Fe, Mg, Na and K in carbonaceous and ordinary chondrites: Geochimica et Cosmochimica Acta, 38, 757–775, doi: 10 .1016 /0016 -7037 (74)90149 -5.

Noriega-Londoño, S., Restrepo-Moreno, S. A., Vinasco, C., Bermúdez, M., Min, K. (2020). Thermochronologic and geomorphometric constraints on the Cenozoic landscape evolution of the Northern Andes: Northwestern Central Cordillera, Colombia. Geomorphology, 351. https://doi.org/10.1016/j.geomorph.2019.106890

Ordóñez-Carmona, O., Valencia, M., Álvarez, M., Sánchez, L., Castaño, L., Echeverri, B. (2005). Metalogenia y evolución tectonomagmatica del distrito minero Segovia-Remedios. X Congreso Colombiano de Geología, Bogotá, Colombia. https://doi.org/10.13140/2.1.4782.8486

Passchier, C., Trouw, R.A. (1996). Microtectonics (2nd ed.). Berlin, Germany: Springer.

Pearce, J,A., Harris, N., Tindle, A. (1984). Trace element discrimination diagrams for the tectonic interpretation of granitic rocks. J. of petrology, v. 25, p 956-983, 1984. C.,

Peccerillo, R., Taylor, S. R., (1976). Geochemistry of Eocene calc-alkaline volcanic rocks from the Kastamonu area, northern Turkey: Contributions to Mineralogy and Petrology, Vol. 58, p. 63-81.

Petrelli, M., Poli, G., Perugini, D., Peccerillo, A. (2005). Petrograph: a New Software to Visualize, Model, and Present Geochemical Data in Igneous Petrology. Geochemistry Geophysics Geosystems, 6(7), Q07011.

Peyton, S. L., Carrapa, B. (2013). An Introduction to Low-temperature Thermochronologic Techniques, Methodology, and Applications. Application of Structural Methods to Rocky Mountain Hydrocarbon Exploration and Development: AAPG Studies in Geology, 15–36. https://doi.org/10.1306/13381688St653578

Pindell, J.L., Kennan, L., Maresch,W.V., Stanek, K.P., Draper, G., Higgs, R. (2005). Plate kinematics and crustal dynamics of circum-Caribbean arc–continent interactions: tectonic controls on basin development in Proto-Caribbean margins. In: Lallemant, A., Sisson, V.B. (Eds.), Caribbean–South American Plate Interactions. Geological Society of

America Special Paper, 394, 7–52.
Reiners, P. (2005). Zircon (U-Th)/He Thermochronometry. In: Reiners, P.W., Ehlers, T.A. (Eds.), Low-temperature thermochronology: Techniques, interpretations and applications (pp. 151–179). Reviews in Mineralogy & Geochemistry.
Reiners, P., Ehlers, T., Zeitler, P. (2005). Past, present, and future of thermochronology. In: Reiners, P.W., Ehlers, T.A. (Eds.), Low-temperature thermochronology: Techniques, interpretations and applications (pp. 1-18). Reviews in Mineralogy & Geochemistry.
Restrepo-Moreno, S. (2009). Long-term morphotectonic evolution and denudation chronology of the Antioqueño Plateau, Cordillera Central, Colombia. Doctorate thesis, University of Florida, U.S.A.
Restrepo, J.J., Toussaint, J.F. (1988). Terranes and continental accretion in the Colombian Andes. In: Episodes, 11, 189–193. https://doi.org/10.18814/epiiugs/1988/v11i3/006
Restrepo, J.J., Toussaint, J.F. (2020). Tectonostratigraphic Terranes in Colombia: An Update, First Part: Continental Terranes. In: Gómez, J., Mateus-Zabala, D. (Eds.). The Geology of Colombia, Volume 1 Proterozoic – Paleozoic. Servicio Geológico Colombiano, Publicaciones Geológicas Especiales 35, 27 pp. Bogotá.
Restrepo-Moreno, S., Foster, D., Bernet, M., Min, K., Noriega, S. (2019). Morphotectonic and Orogenic Development of the Northern Andes of Colombia: A Low-Temperature Thermochronology Perspective. In: Cediel, F., Shaw, P (Eds.). Geology and Tectonics of Northwestern South America. (pp. 749-832). Frontiers in Earth Sciences.
Rodriguez, J., Pernet, A. (1983). Recursos Minerales de Antioquia. Boletin Geologico Ingeominas, 26(3), 72.
Rusell. (1959). Secuence of Fissures Frontino Area. Internal Report Frontino Gold mines, Segovia, 2.
Saenz, E. A. (2003). Fission track thermochronology and denudational response to tectonics in the north of The Colombian Central Cordillera. School of Science, 138.
Sánchez, L., Ordóñez-Carmona, O., Castaño, L. (2007). Revisión de modelos de fracturamiento y controles estructurales como guías de exploración de filones auríferos en el Distrito Minero Segovia Remedios. Bolentín Ciencias de la Tierra, 21, 49-58.
Sarmiento-Rojas, L., Van Wess, J., Cloetingh, S. (2006). Mesozoic transtensional basin history of the Eastern Cordillera, Colombian Andes: Inferences from tectonic models. Journal of South American Earth Sciences, 21(4), 383–411. https://doi.org/10.1016/j.jsames.2006.07.003
Shaw, R., Leal-Mejía, H., Melgarejo, J. (2019). Phanerozoic Metallogeny in the Colombian Andes: A Tectono-magmatic Analysis in Space and Time. In: Cediel, F., Shaw, P (Eds.). Geology and Tectonics of Northwestern South America. (pp. 411-549). Frontiers in Earth Sciences.
Sillitoe, R. (2008). Special paper: Major Gold Deposits and belts of the North and South American Cordillera: Distribution, tectonomagmatic settings, and metallogenic considerations. Economic Geology, 103(4), 663–687. https://doi.org/10.2113/gsecongeo.103.4.663
Spikings, R., Cochrane, R., Villagomez, D., Van der Lelij, R., Vallejo, C., Winkler, W., & Beate, B. (2015). The geological history of northwestern South America: from Pangaea

to the early collision of the Caribbean Large Igneous Province (290–75 Ma). Gondwana Research.

SRK Consulting. (2018). Amended NI 43-101 technical report prefeasibility study update Segovia Project Colombia. Report prepared for Gran Colombia Gold, Canada. 328 pp.

Streckeisen, A. (1976). To each plutonic rock its proper name: Earth Science Reviews, Vol. 12, p. 1-33.

Tremmlet. (1955). The Fracture Pattern and Structural controls of ore localization at Frontino Gold Mines. Internal Report. Frontino Gold mines, Segovia, 15.

Tschanz, C.M., Marvin, R.F., Cruz, J., Mehnert, H.H., Ce- bula, G.T. (1974). Geologic evolution of the Sierra Nevada de Santa Marta, northeastern Colombia. Geological Society of America Bulletin, 85(2), 273–284.

Van der Hammen, T. (1961). Late Cretaceous and Tertiary stratigraphy and tectogenesis of the Colombian Andes: Geologie en Mijnbouw, 40, 181-188.

Villagómez, D., Spikings, R., Magna, T., Kammer, A., Winkler, W., Beltrán, A. (2011). Geochronology, geochemistry and tectonic evolution of the Western and Central cordilleras of Colombia. Lithos, 125(3–4), 875–896. https://doi.org/10.1016/j.lithos.2011.05.003

Villagómez, D., Spikings, R. (2013). Thermochronology and tectonics of the Central and Western Cordilleras of Colombia: Early Cretaceous-Tertiary evolution of the Northern Andes. Lithos, 160-161, 228-249. https://doi.org/10.1016/j.lithos.2012.12.008

Vinasco, C., Cordani, U., González, H., Weber, M., Pelaez, C. (2006). Geochronological, isotopic, and geochemical data from Permo-Triassic granitic gneisses and granitoids of the Colombian Central Andes. Journal of South American Earth Sciences, 21(4), 355–371. https://doi.org/10.1016/j.jsames.2006.07.007

White, W. (2013). Decay systems and geochronology I. In: Isotope Geochemistry (pp. 32-72). Wiley-Blackwell.

Wolf, R.A., Farley, K. A., Kass, D.M. (1998). A sensitivity analysis of the apatite (U-Th)/He thermochronometer. Chemical Geology, 148, 105-114.

Wood, D. A. (1979). A variability veined sub-oceanic upper mantle-genetic significance for mid ocean ridge basalts from geochemical evidence. Geology, 7, 499-503.

Wood, D., Hedenquist, J. (2019). Mineral Exploration: Discovering and Defining Ore Deposits. SEG Newsletter, 116, 11-22.

Zindler, A., Hart, S. (1986). Chemical Geodynamics. Annual Review of Earth and Planetary Sciences, 14, 493-571

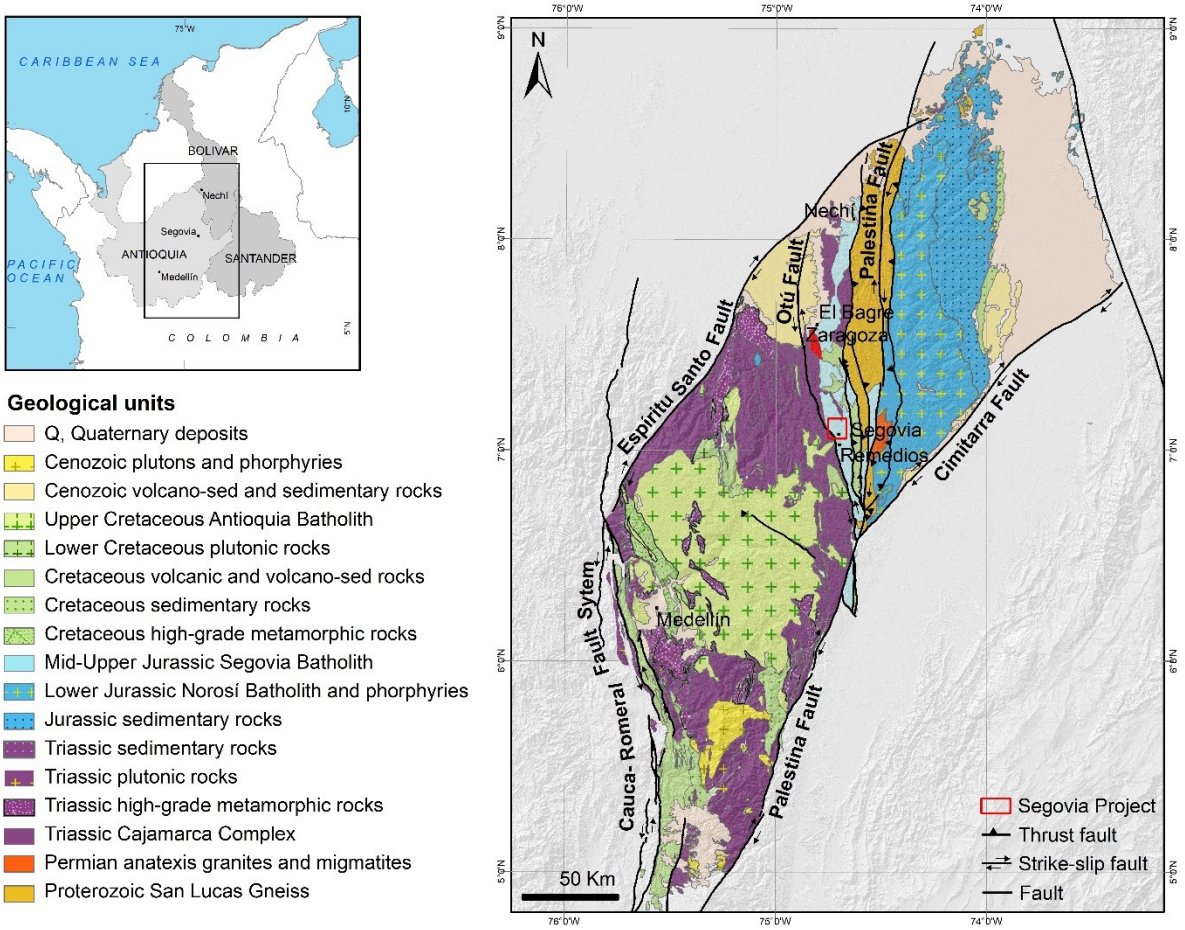

FIGURE 1. Regional geological map showing the main chronostratigraphic units and faults in the northern Central Cordillera (modified from Gómez et al., 2015). The red polygon corresponds to the Segovia mining project.

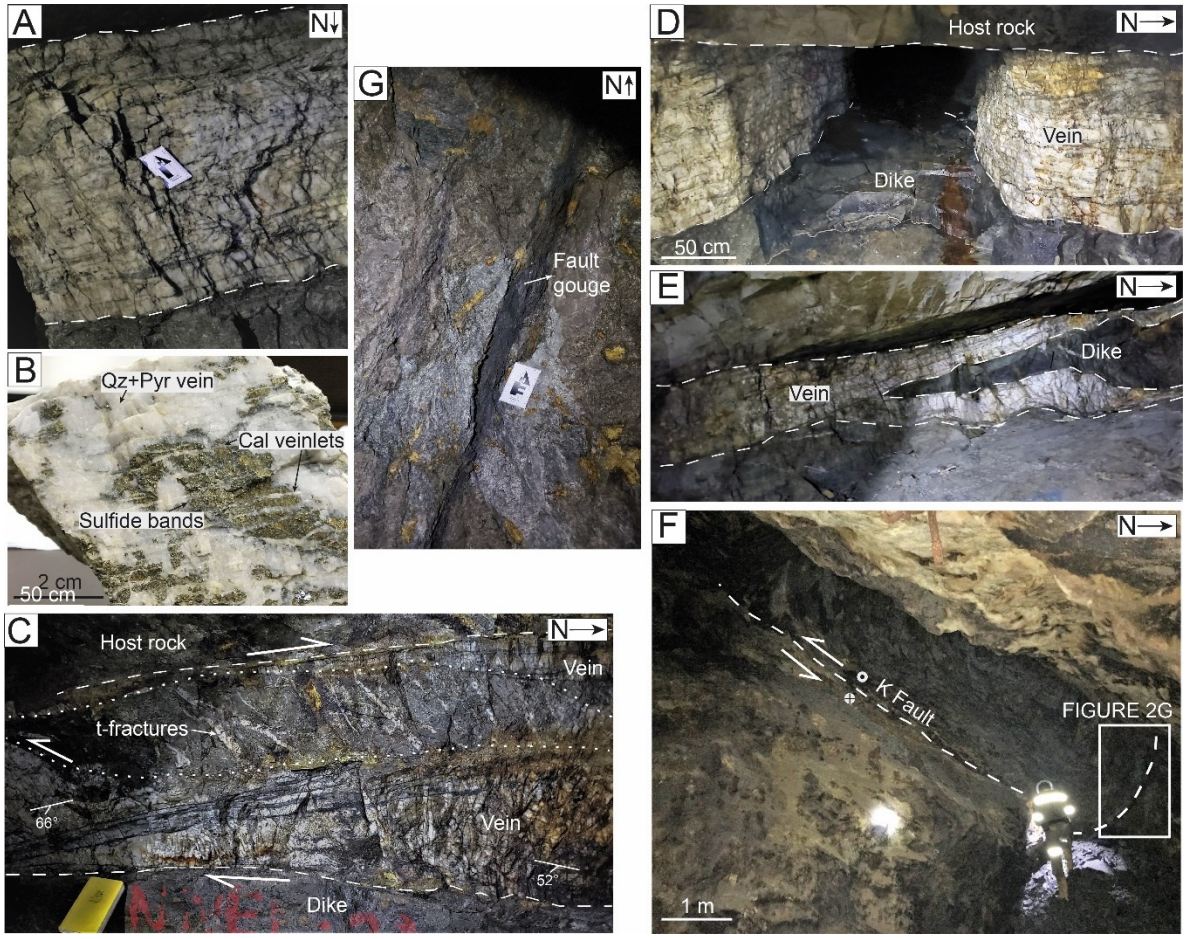

FIGURE 2. Ore deposit field characteristics in the Segovia Project. **A)** Main vein in El Silencio Mine "Veta Manto" showing a typical thickness of 1.2 m. **B)** Representative hand-sample from a quartz-pyrite vein with sulfide bands cut by calcite veinlets. **C)** En-echelon tension fractures within the El Silencio Vein reflecting NW-oriented maximum shear. **D)** Mafic dikes placed in the vein footwall and **E)** between the vein. **F)** Outcrop of the K Fault in the El Silencio Mine truncating the vein. Slickenslides on the fault plane indicate inverse-sinistral movement. **G)** Close-up of the K Fault displaying fault gouge bands.

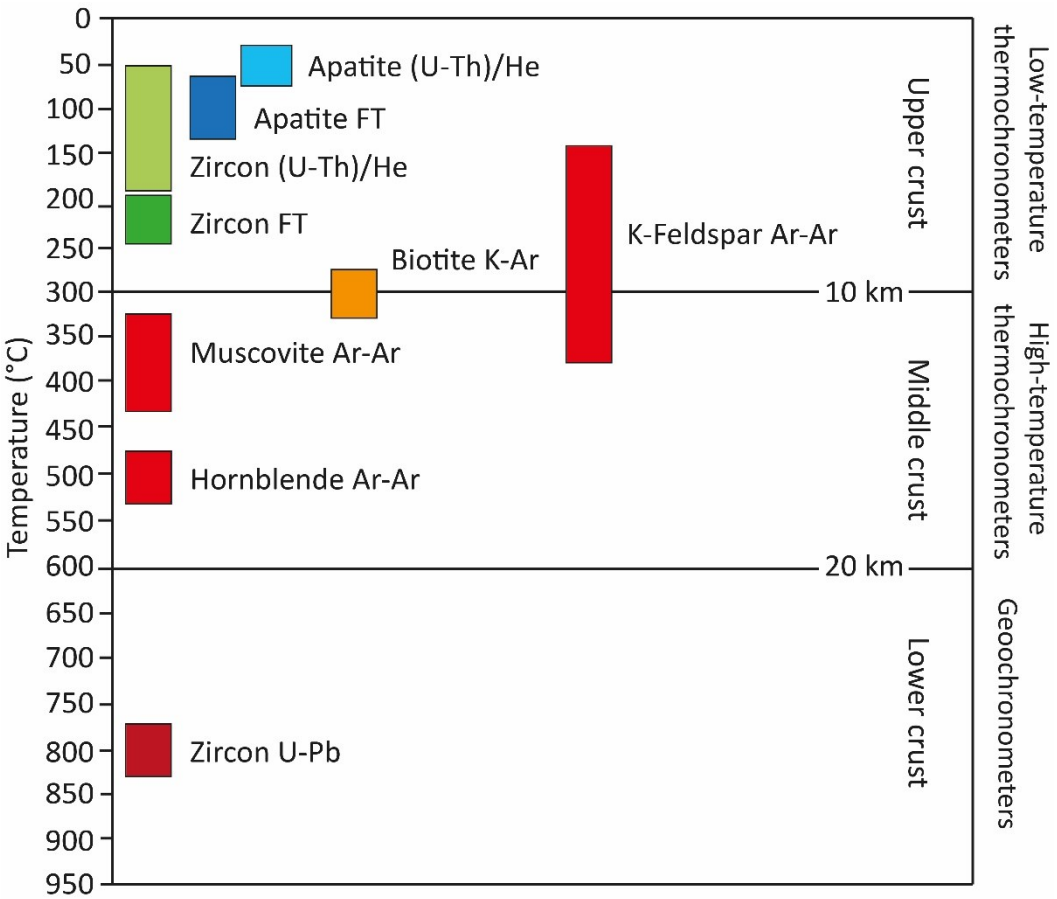

FIGURE 3. Common geochronological and thermochronological dating systems and their sensitive temperature ranges (modified from Bernet at al., 2019).

Sample	X	Y	Mine	Rock name	Q	A	P
SE-01	930940	1276768	Cristales	Granodiorite	29	12	59
SE-02	930822	1276828	Cristales	Monzogranite	23	34	43
SE-06	931366	1276197	El Silencio	Granodiorite	50	6	44
SE-08	931216	1276044	El Silencio	Granodiorite	36	21	44
SE-11	930536	1272949	Providencia	Monzogranite	26	35	38
SE-14	930302	1272736	Providencia	Tonalite	35	12	53

TABLE 1. Petrographic data of the Segovia Batholith and modal QAP calculations.

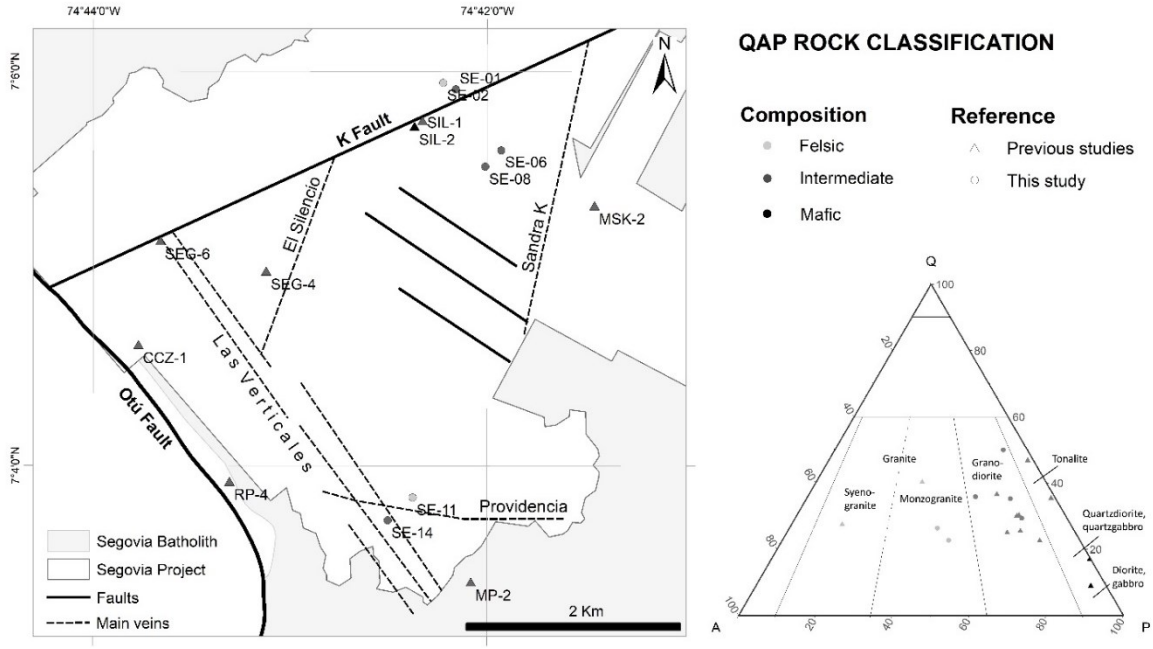

FIGURE 4. Distribution of petrographic samples with modal analyses in the Segovia Project. QAP classification diagram after Streckeisen (1976). Data from previous studies is represented in triangles (Álvarez et al., 2007; González et al., 2010; Álvarez, 2013).

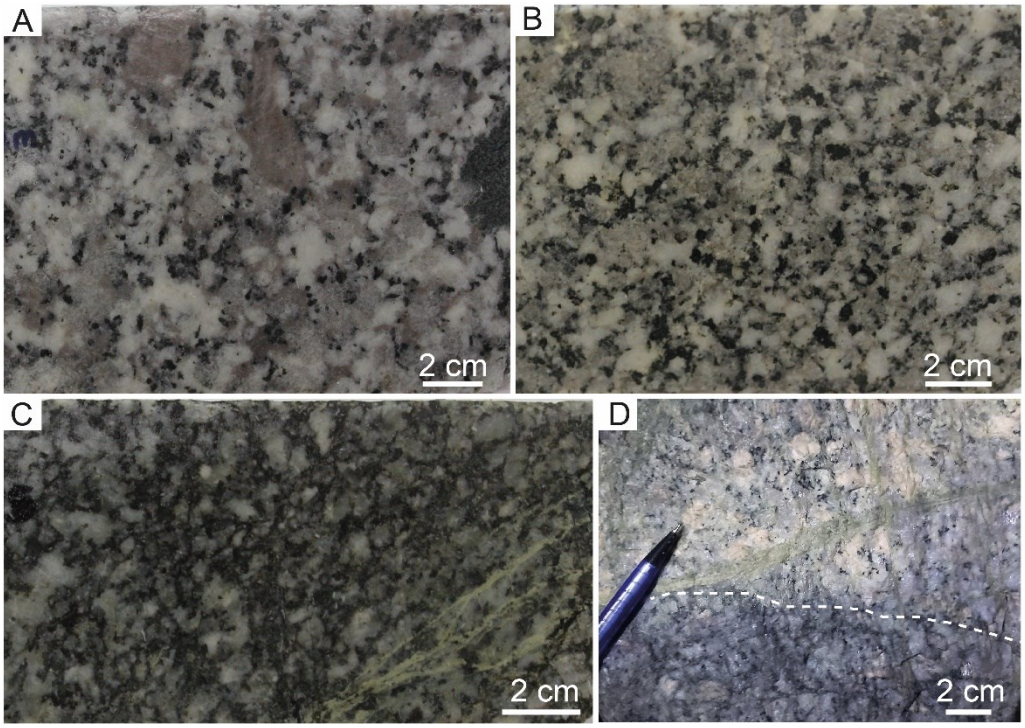

FIGURE 5. Hand-sample scale characteristics of the Segovia Batholith in the Segovia Project. **A)** Pegmatitic texture with 2 cm-large K-felspar crystals (sample SE-02). **B)** Typical coarse-grained phaneritic texture (sample SE-11). **C)** Fine-grained phaneritic texture with secondary biotite and chlorite veinlets (sample SE-14). **D)** Gradational contact in El Silencio Mine from K-felspar-rich pegmatitic facies to plagioclase-rich phaneritic facies.

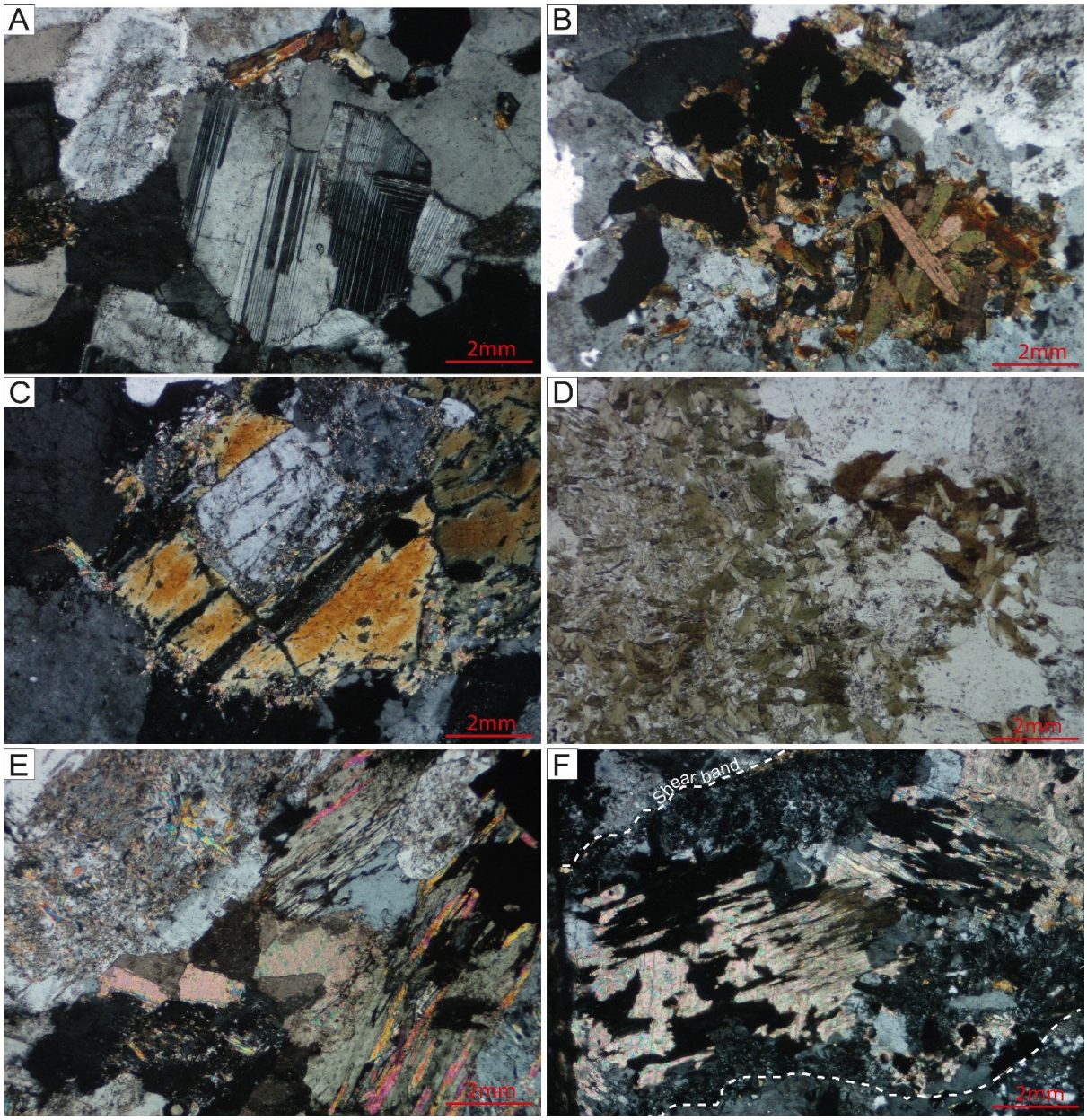

FIGURE 6. Thin section microphotographs of the Segovia Batholith. **A)** Typical section of unaltered rock with hypidiomorphic fabric and phaneritic texture composed mainly of plagioclase, K-feldspar, quartz, and minor biotite (sample SE-02). **B)** Sample SE-08 with biotite glomerocrysts. **C)** Sample SE-11 with sericitic alteration replacing plagioclase along cleavage favored by grain contact with biotite. **D)** Sample SE-08 showing transition from primary brown biotite to secondary green biotite. **E)** Sample SE-06 displaying propylitic alteration with Chl+Ep+Cal replacing plagioclase and biotite. **F)** Sample SE-14 with micro shear bands containing sulfides replacing calcite pseudomorphs after biotite.

Element	Location	X	Y	Strike	Dip	DD
Vein	El Silencio Mine	930643	1276471	15	52	E
Vein	El Silencio Mine	930643	1276471	354	66	E
t-fracture	El Silencio Mine	930643	1276471	310	40	E
t-fracture	El Silencio Mine	930643	1276471	320	30	E
Vein	Providencia Mine	931093	1272872	270	30	N
Vein	Providencia Mine	931093	1272872	278	30	E
t-fracture	Providencia Mine	931093	1272872	356	28	E
t-fracture	Providencia Mine	931093	1272872	5	44	E

DD=Dip Direction

TABLE 2. Structural data obtained in the Segovia Project.

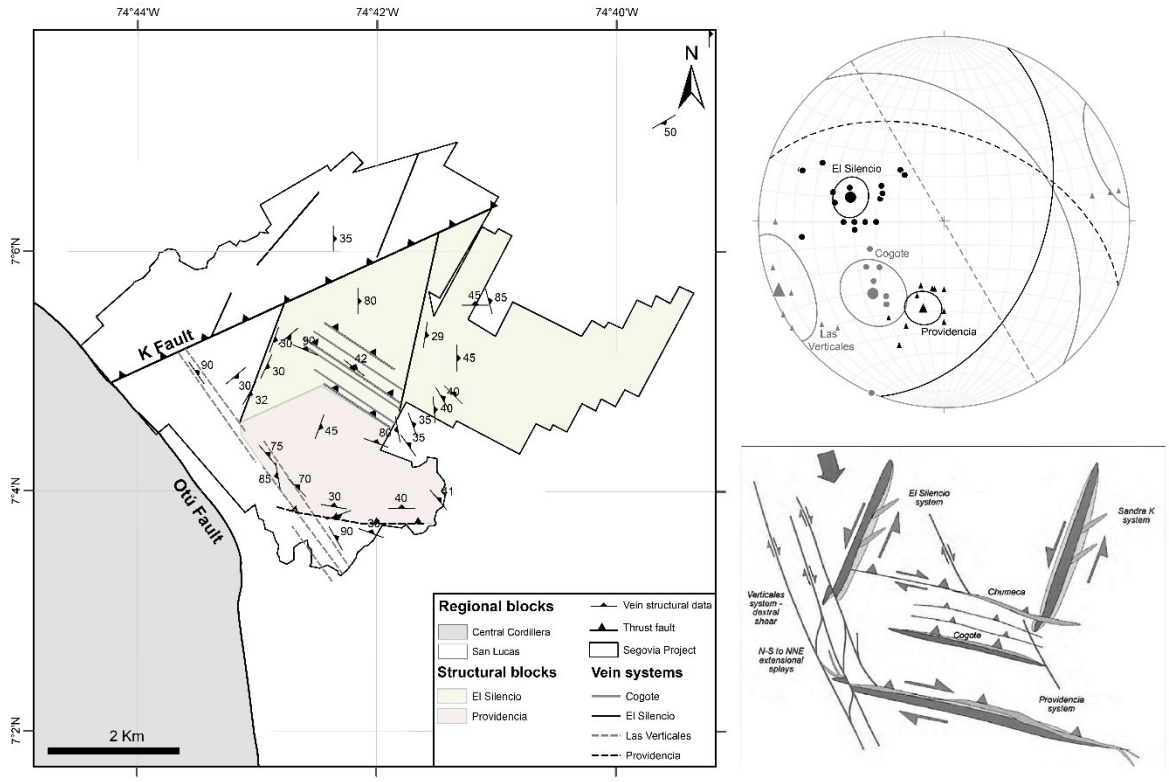

FIGURE 7. Structural map of the Segovia Project with proposed division in structural blocks. Stereonet on the upper right shows the poles and mean trace of each vein system, constructed from secondary (Echeverri, 2006; Echeverry et al., 2009; González et al., 2010; SRK Consulting, 2018) and primary data. The structural model on the bottom right is modified from SRK Consulting (2018) and shows shear and stress tensor relations in the syn-mineralization stage.

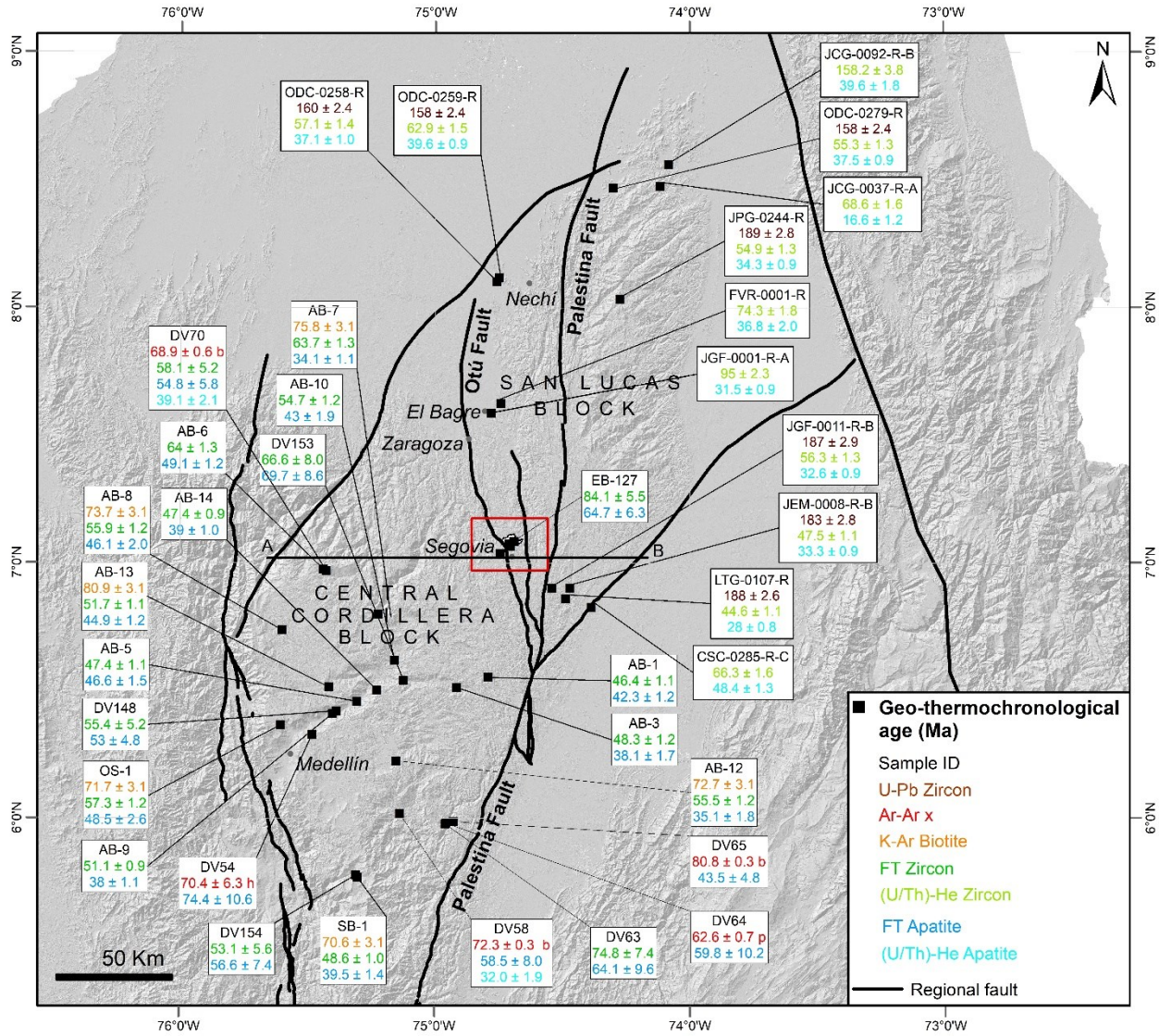

FIGURE 8. Compiled geo and thermochronological data at a regional scale for two lithotectonic blocks in the northern Central Cordillera. The red polygon corresponds to the location of the Segovia Project. Data compiled from Central Cordillera Block (Saenz, 2003; Ibanez-Mejía et al., 2007; Restrepo; 2009; Leal-Mejía, 2011; Villagómez and Spikings, 2013). Data compiled from San Lucas Block (Echeverri, 2006; Leal-Mejía, 2011; Caballero et al., 2013; Noriega-Londoño, in review).

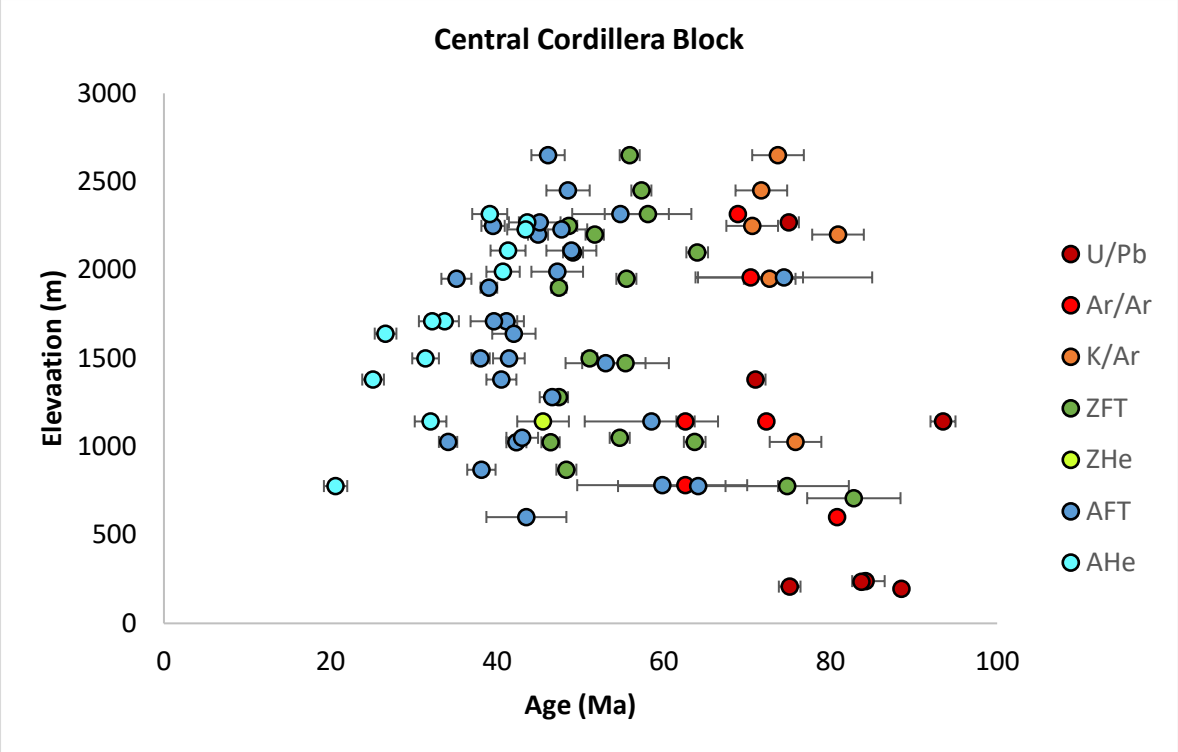

FIGURE 9. AER profile of the Central Cordillera Block. Three cooling intervals are identified in the Late Cretaceous-early Paleocene, late Paleocene-Eocene, and Oligocene.

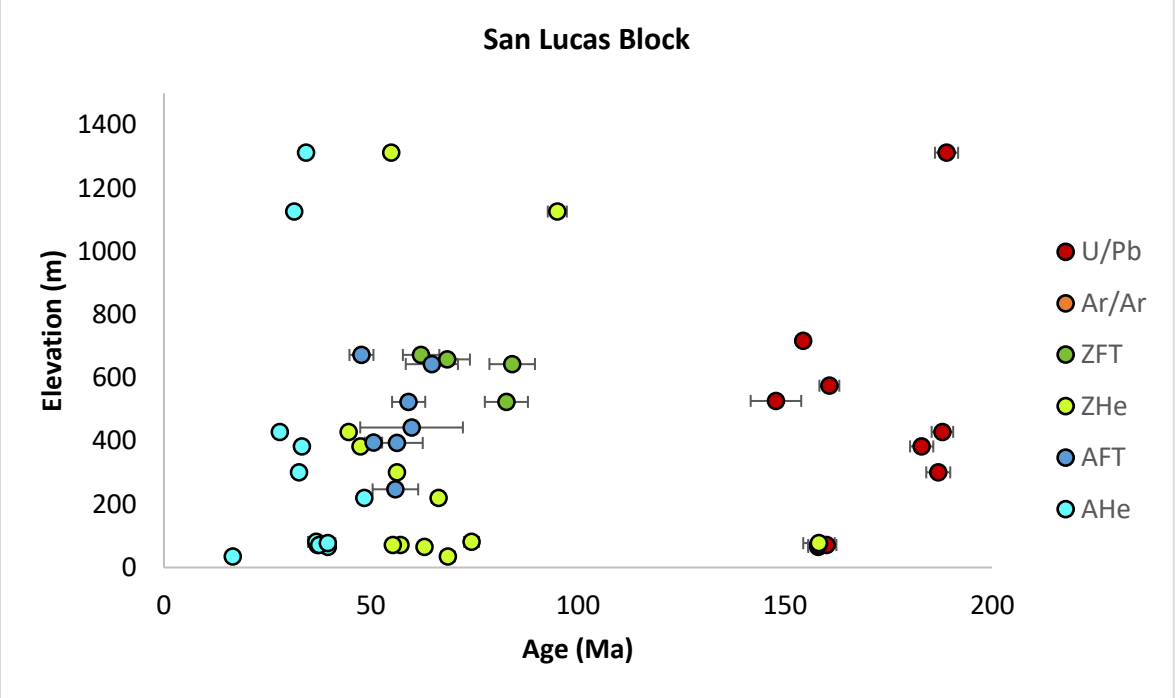

FIGURE 10. AER profile of the San Lucas Block. Two cooling periods are identified in the Late Cretaceous-early Eocene and Eocene-Miocene. Notice the negative trend in the profile, with ages becoming younger with altitude.

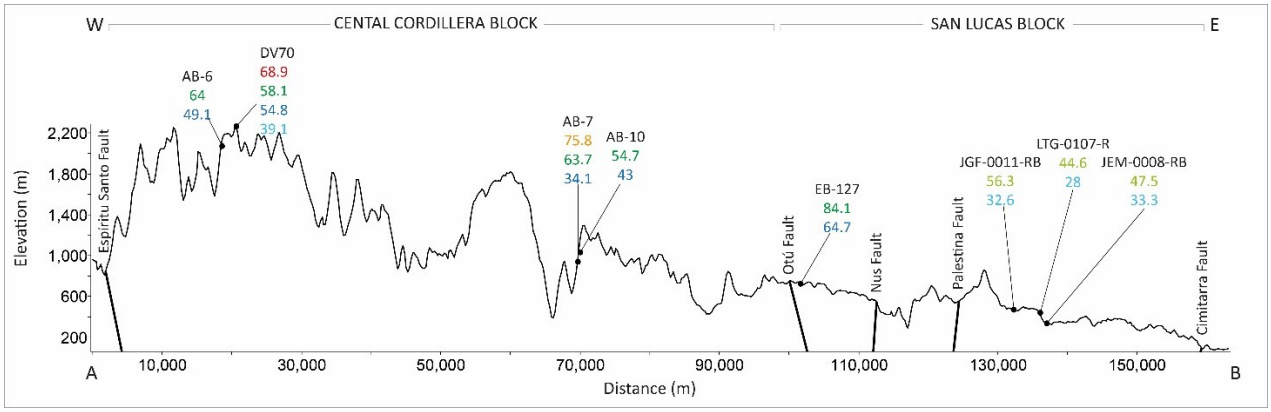

FIGURE 11. Topographic profile of the section A-B in figure 8. Higher elevation is apparent in the Central Cordillera Block compared to the shallower San Lucas Block. Notice, however, different age intervals at similar elevations.

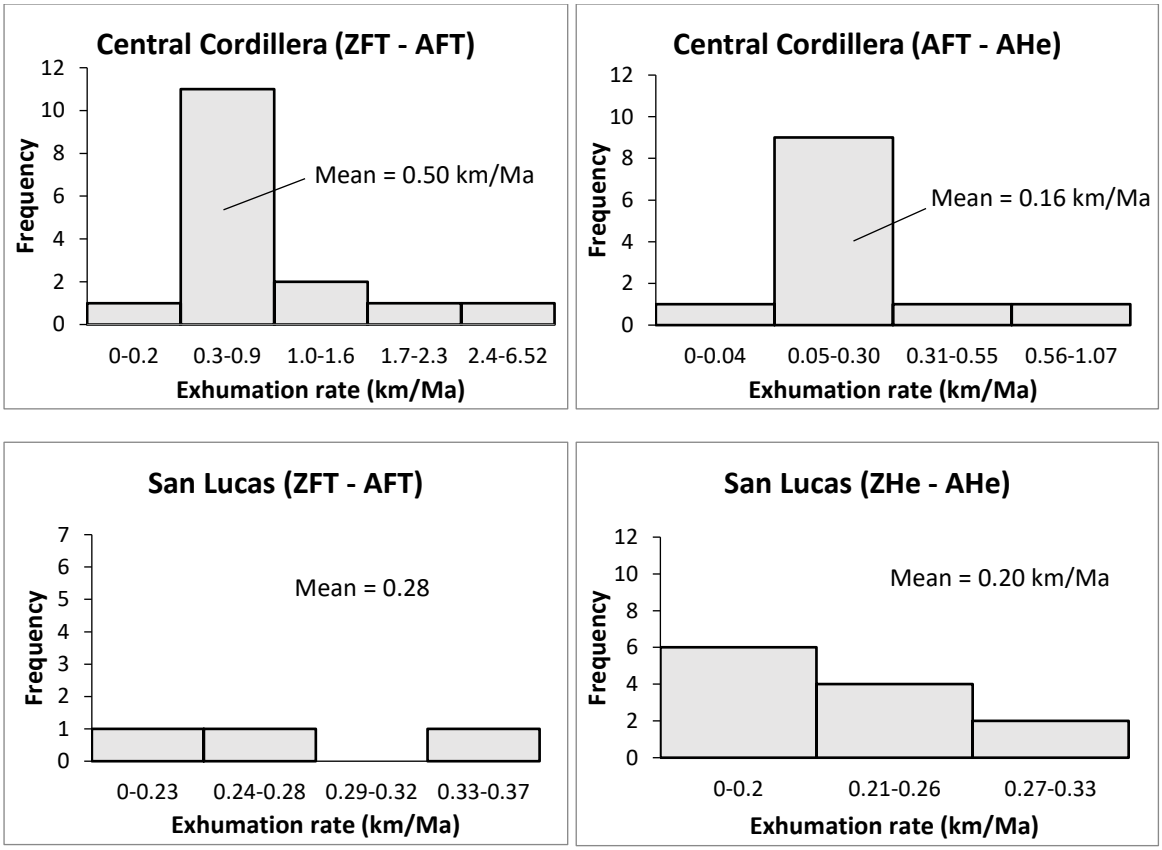

FIGURE 12. Histograms showing frequency intervals of exhumation rates calculated for each sample between different dating systems. In the Central Cordillera Block, the indicated interval corresponds to the one selected for modeling. Notice higher exhumation mean rates in the Central Cordillera Block for the ZFT-AFT systems temperature-depth interval.

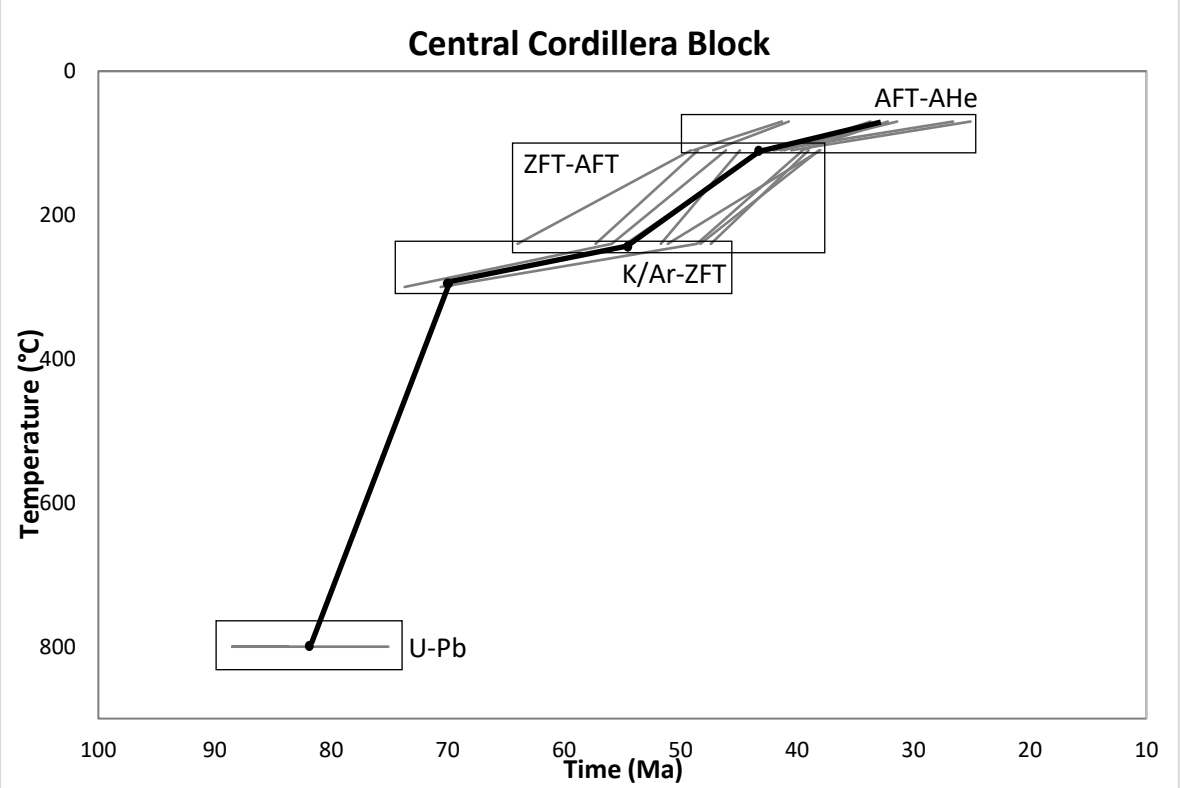

FIGURE 13. T-t model constructed for the Central Cordillera Block. The black boxes indicate the system used to constrain the corresponding temperature interval. The bold black line at the center corresponds to the interpreted trajectory. U-Pb data (Ibanez-Mejía, 2007; Leal-Mejia, 2011), K/Ar-ZFT data (Saenz, 2003), ZFT-AFT data (Saenz, 2003; Villagómez and Spikings, 2013), AFT-AHe data (Restrepo, 2009; Villagomez and Spikings, 2013).

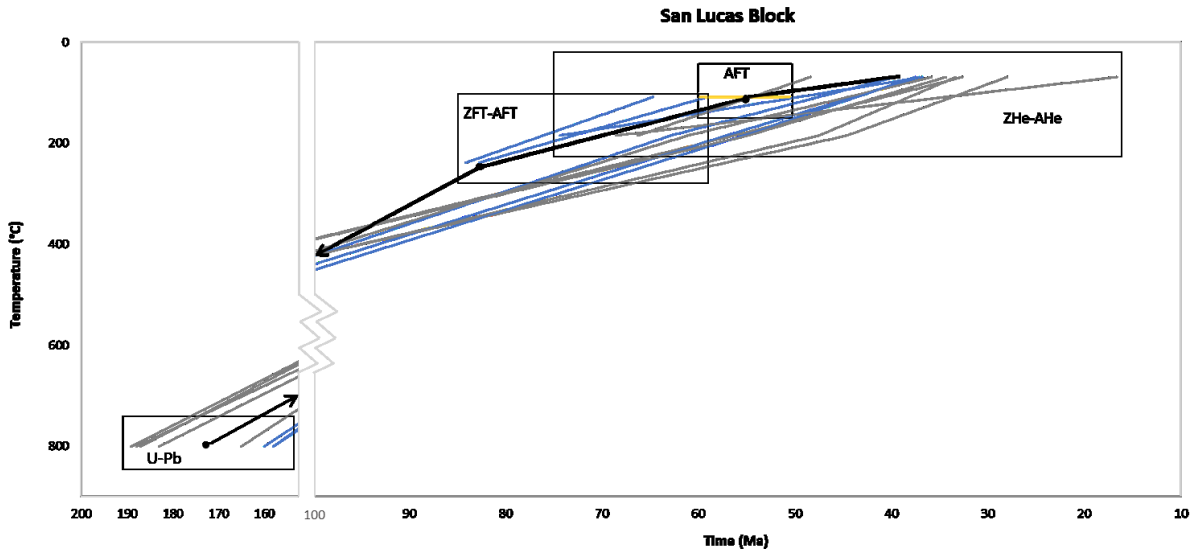

FIGURE 14. T-t model constructed for the San Lucas Block. The black boxes indicate the system used to constrain the corresponding temperature interval (data from Leal-Mejía, 2011: U-Pb; Echeverri, 2006: ZFT-AFT; Noriega-Londoño, in review: ZHe-AHe). The yellow line corresponds to samples with only AFT data (Caballero et al., 2013). The blue lines correspond to samples taken west of the Palestina fault, the gray lines to samples taken east. The bold black line at the center corresponds to the interpreted trajectory.

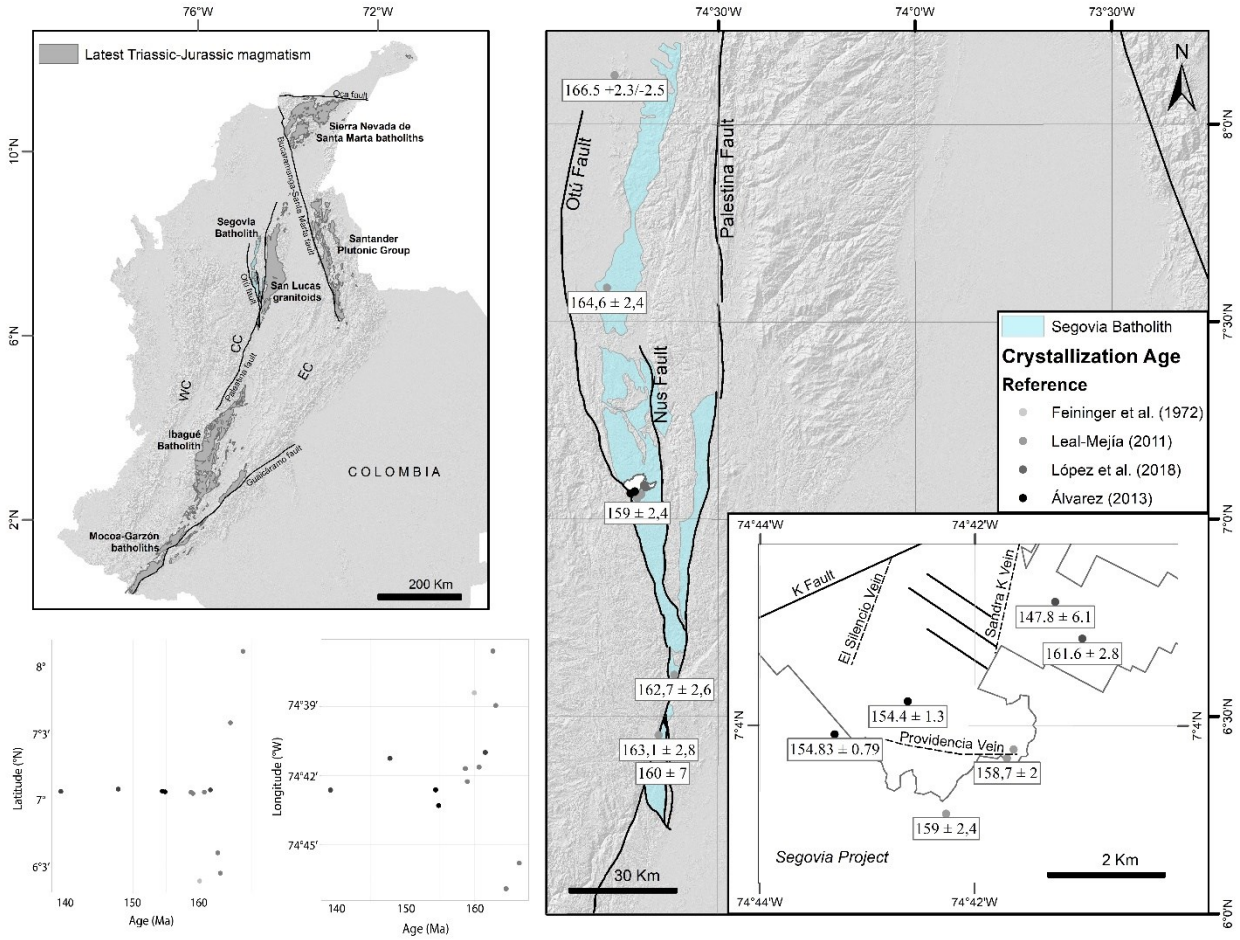

FIGURE 15. Distribution of crystallization ages in the Segovia Batholith and close-up to the Segovia Project (data compiled from Feininger et al., 1972; Leal-Mejía, 2011; López et al., 2018; Álvarez, 2013). An overview of this distribution shows random variations with latitude, but a west-younging trend with longitude.

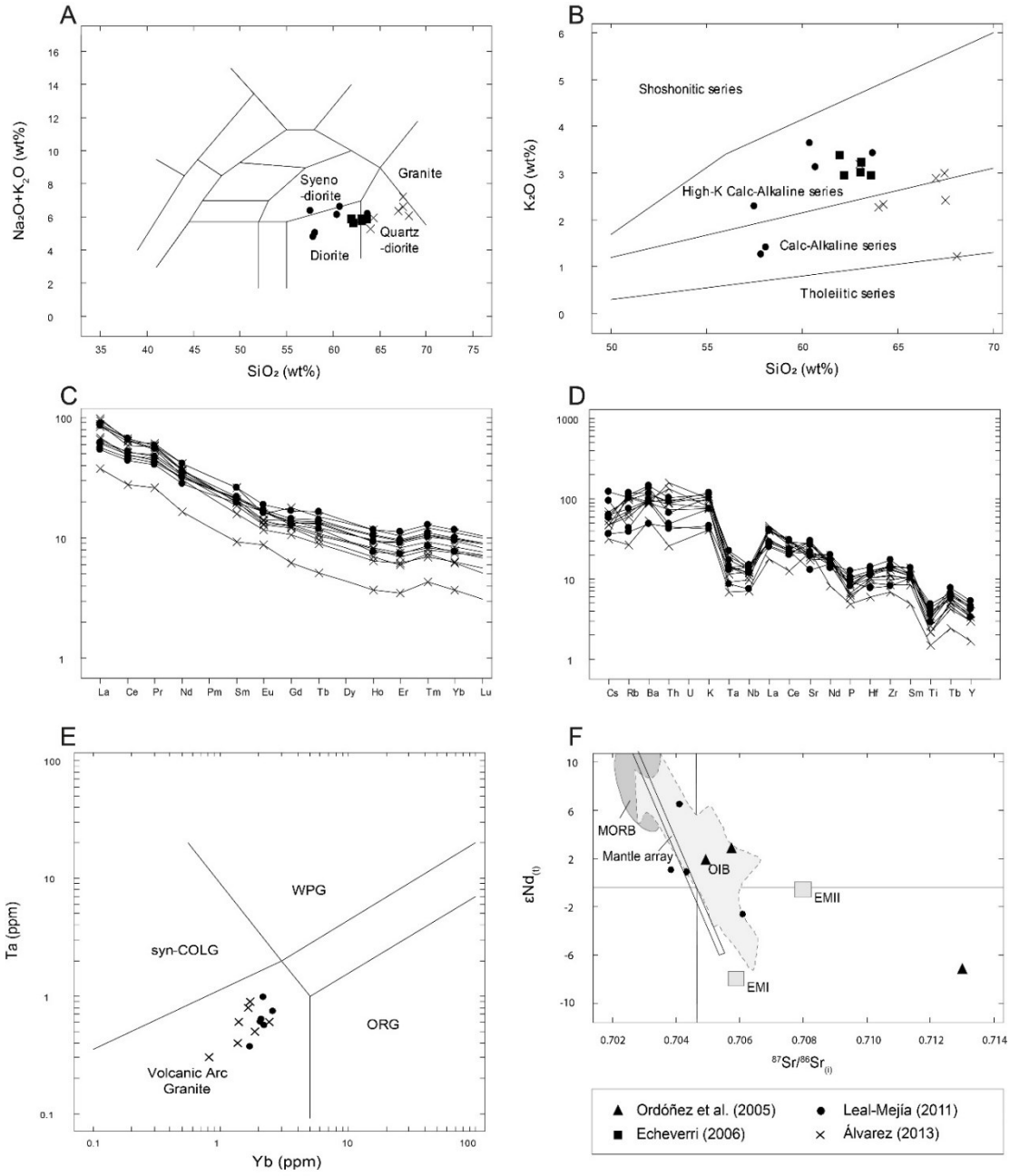

FIGURE 16. Geochemical and isotopic signature of the Segovia Batholith compiled from previous studies (Ordóñez et al, 2005; Echeverri, 2006; Leal-Mejía, 2011; Álvarez, 2013). **A)** TAS classification diagram (after Cox et al., 1979). **B)** K_2O vs. SiO_2 diagram (after Peccerrillo and Taylor, 1976). **C)** Multi-element diagram chondrite-normalized (after Nakamura, 1974). **D)** Spider diagram PRIMA-normalized (after Wood et al., 1979). **E)** Ta vs. Yb tectonic affinity diagram (after Pearce et al., 1984). **F)** εNd vs. Sr/Sr reservoir diagram (after Zindler and Hart,1986).

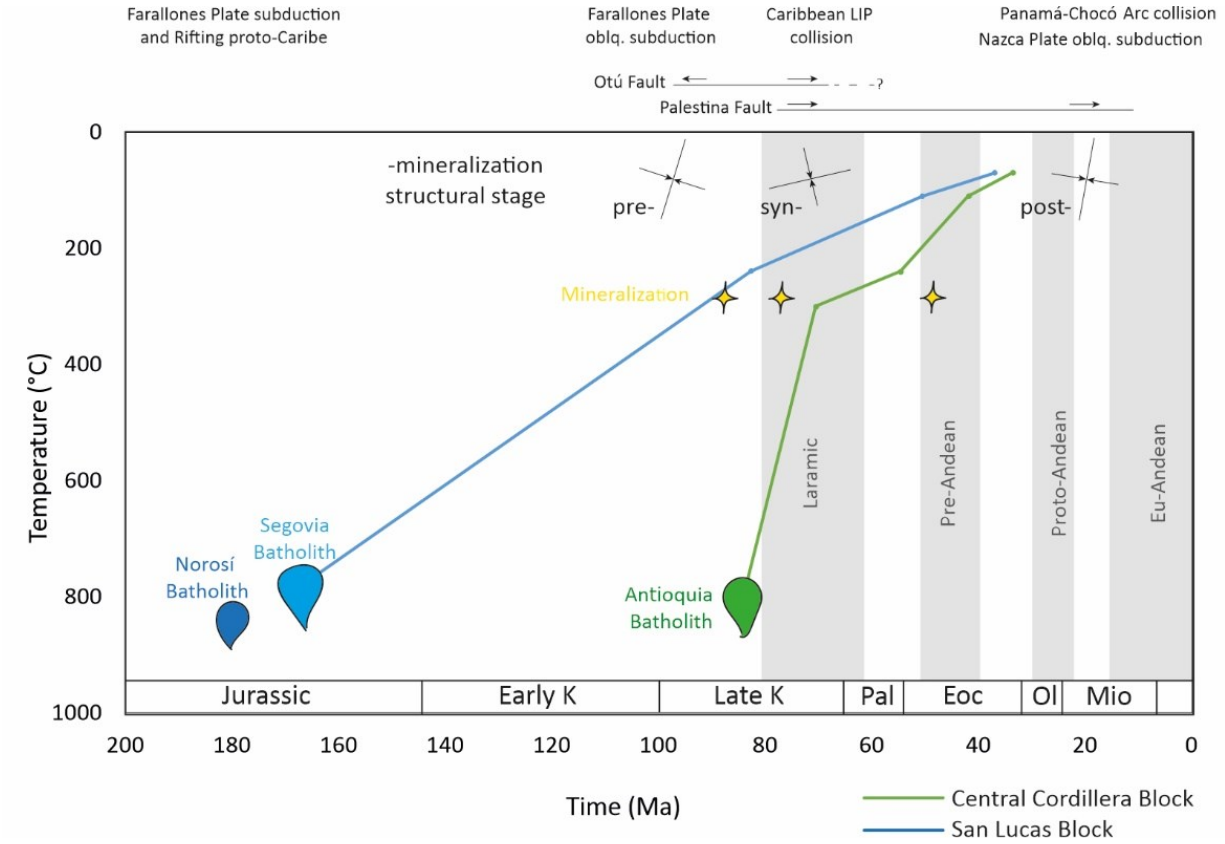

FIGURE 17. Compilation of the interpreted T-t trajectories for the San Lucas and Central Cordillera blocks, with tectonic events of the northern Andes (compiled in Cediel et al., 2019), fault activity of the Otú (Feininger et al., 1972) and Palestina (Feininger, 1970; Collins et al., 1981) faults. Structural stages are drawn based on the analysis discussed in section 6.4. Yellow stars correspond to Late Cretaceous mineralization ages (Leal-Mejía, 2011; López et al., 2018), plus an Eocene hydrothermal event constrained by AFT (Echeverri, 2006). Highlighted gray polygons correspond to the orogenic phases of Van der Hammen (1961).

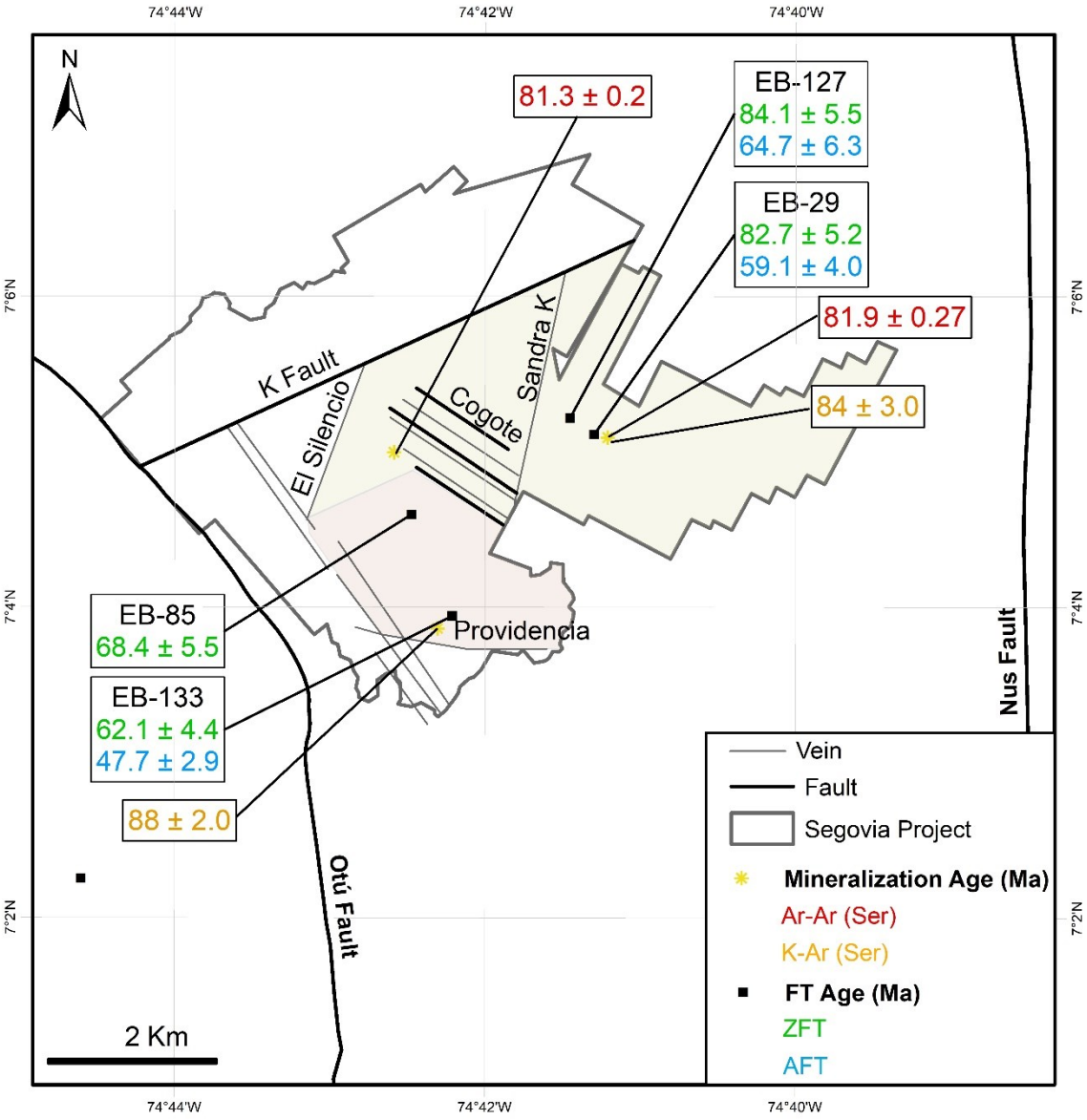

FIGURE 18. Close-up of the red polygon in figure 8, showing the distribution of local thermochronological data in the Segovia Project (data from Echeverri, 2006). The T-t trajectories correspond to the El Silencio Block (top), and Providencia Block (bottom), with the same colors indicated on the map for ZFT and AFT systems. The timing of mineralization corresponds to Ar-Ar and K-Ar ages (Leal-Mejía, 2011; López et al., 2018). Notice the greater thermal gradient in the El Silencio Block between mineralization at about 400°C and cooling of the ZFT system at 240°C.

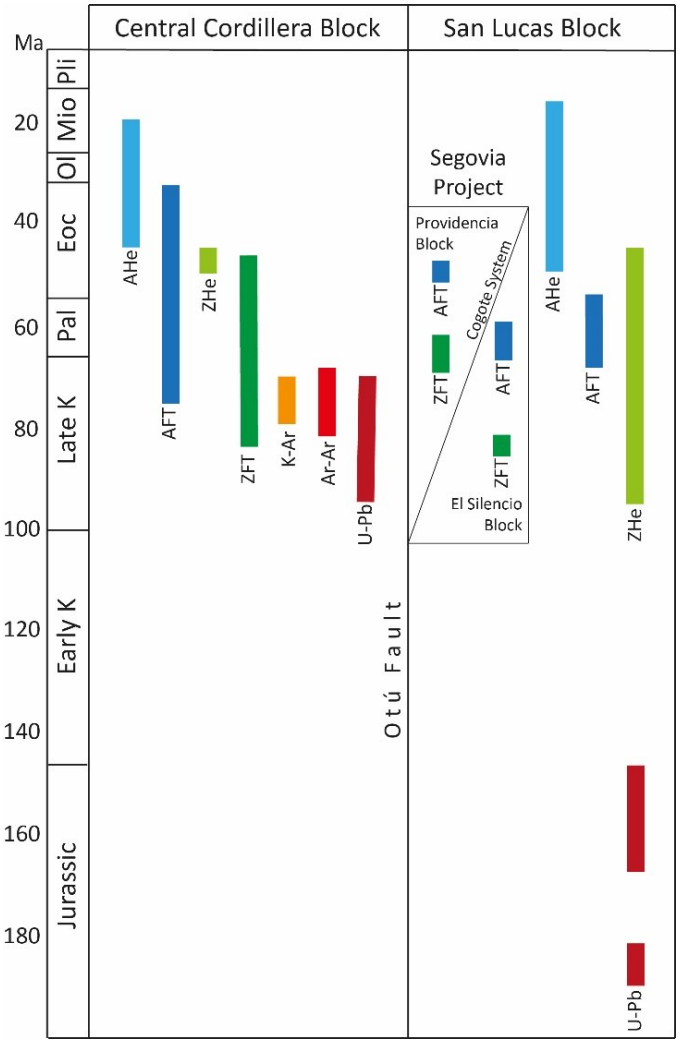

FIGURE 19. Compilation of age intervals indicated by each geo-thermochronometer in the regional and local blocks. Data compiled for the Central Cordillera Block (Saenz, 2003; Restrepo; 2009; Leal-Mejía, 2011; Villagómez and Spikings, 2013), and San Lucas Block (Leal-Mejía, 2011; Echeverri, 2006; Caballero et al., 2013; Noriega-Londoño, in review).